Filamentous morphology of bacteria delays the timing of phagosome morphogenesis in macrophages

Akriti Prashar,[1,3] Sonam Bhatia,[3] Darren Gigliozzi,[1,3] Tonya Martin,[3] Carla Duncan,[4] Cyril Guyard,[2,4] and Mauricio R. Terebiznik[1,3]

[1]Department of Cell and Systems Biology, University of Toronto, Toronto, Ontario M5S 3G5, Canada
[2]Department of Laboratory Medicine and Pathobiology, University of Toronto, Toronto, Ontario M5S 1A8, Canada
[3]Department of Biological Sciences, University of Toronto at Scarborough, Toronto, Ontario M1C 1A4, Canada
[4]Ontario Agency for Health Protection and Promotion, Toronto, Ontario M5G 1V2, Canada

Although filamentous morphology in bacteria has been associated with resistance to phagocytosis, our understanding of the cellular mechanisms behind this process is limited. To investigate this, we followed the phagocytosis of both viable and dead *Legionella pneumophila* filaments. The engulfment of these targets occurred gradually and along the longitudinal axis of the filament, therefore defining a long-lasting phagocytic cup stage that determined the outcome of phagocytosis. We found that these phagocytic cups fused with endosomes and lysosomes, events linked to the maturation of phagosomes according to the canonical pathway, and not with the remodeling of phagocytic cups. Nevertheless, despite acquiring phagolysosomal features these phagocytic cups failed to develop hydrolytic capacity before their sealing. This phenomenon hampered the microbicidal activity of the macrophage and enhanced the capacity of viable filamentous *L. pneumophila* to escape phagosomal killing in a length-dependent manner. Our results demonstrate that key aspects in phagocytic cup remodeling and phagosomal maturation could be influenced by target morphology.

Introduction

Professional phagocytes engulf and degrade a large variety of materials including apoptotic bodies, microbes, and abiotic particles that enter the organism, thus playing key roles in the establishment of the immunological response and in tissue homeostasis and remodeling (Aderem and Underhill, 1999; Flannagan et al., 2012). Phagocytosis is triggered by the attachment of target particles to phagocytic receptors. Their activation induces the development of F-actin–enriched pseudopodia that engulf the target into a phagocytic cup that seals and separates from the plasma membrane to form a phagosome (Flannagan et al., 2012). Phagocytic cups and phagosomes undergo complex remodeling and maturation through highly coordinated, spatiotemporally regulated mechanisms. Through sequential fusion with early and late endosomes and lysosomes, the newly formed phagosomes acidify and acquire hydrolytic properties, which ultimately degrade their cargo (Vieira et al., 2002).

Different phagocytic receptors can recognize targets of diverse molecular nature and respond by triggering distinctive uptake mechanisms, modulating phagosome maturation and/or the immune response (Underhill and Goodridge, 2012). While phagocytes encounter targets of disparate morphology, i.e., pathogens ranging from protozoa and filamentous molds to yeast and bacteria, how this variable affects the outcome of phagocytosis has been largely overlooked (Champion and Mitragotri, 2006; Justice et al., 2008). Only in recent years have studies begun to demonstrate that morphology can affect phagocytosis, albeit through mechanisms that remain poorly understood. With implications for designing drug-delivery carriers, studies using engineered polystyrene particles of varying shapes have demonstrated that filamentous targets can only be ingested if they are engaged by the macrophages through their poles

Correspondence to Mauricio R. Terebiznik: terebiznik@utsc.utoronto.ca

Abbreviations used in this paper: DQ-ova, DQ-ovalbumin; FBT, filamentous bacterial target; GPI, glycosyl phosphatidylinositol; LAMP1, lysosomal-associated membrane protein 1; LCV, *Legionella*-containing vacuole; *Lp*, *Legionella pneumophila*; PI3K, phosphatidylinositol 3′-kinase; PI(4,5)P2, phosphatidylinositol-4,5-bisphosphate; RBC, red blood cell; S-FBT, *Salmonella* filamentous bacterial target; T-PC, tubular phagocytic cup.

© 2013 Prashar et al. This article is distributed under the terms of an Attribution–Noncommercial–Share Alike–No Mirror Sites license for the first six months after the publication date (see http://www.rupress.org/terms). After six months it is available under a Creative Commons License (Attribution–Noncommercial–Share Alike 3.0 Unported license, as described at http://creativecommons.org/licenses/by-nc-sa/3.0/).

The Rockefeller University Press $30.00
J. Cell Biol. Vol. 203 No. 6 1081–1097
www.jcb.org/cgi/doi/10.1083/jcb.201304095

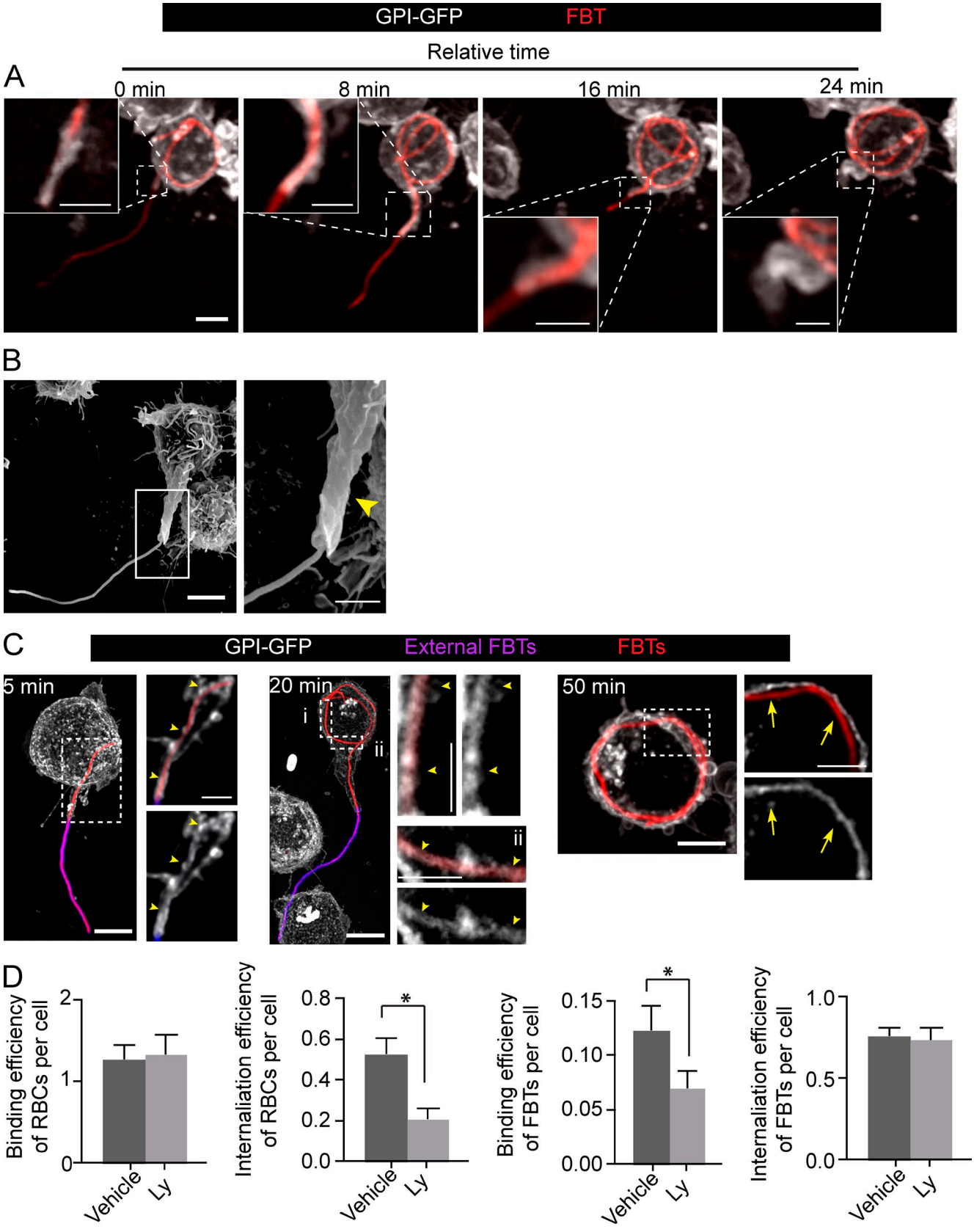

Figure 1. **Uptake of bacterial filaments occurs through a tubular phagocytic cup.** (A) Phagocytosis of FBTs by GPI-GFP expressing RAW macrophage. Frames from a time-lapse sequence depict the T-PC extending and engulfing the FBT after 15 min of phagocytosis (T0). Insets show higher magnification of framed regions. (B) Scanning electron micrograph of RAW cell showing the T-PC (arrowhead) formed after 20 min of phagocytosis. (C) T-PCs remain positive for GPI until the FBTs are fully internalized. Phagocytosis was allowed to proceed to indicated times, cells fixed, and external FBTs were immunolabeled (pink). For each time point, panels on the right are magnified single planes from framed regions. GPI-GFP–positive T-PCs (arrowheads) and loss of

(Champion et al., 2007; Champion and Mitragotri, 2006, 2009; Sharma et al., 2010). In agreement with this, the uptake of filamentous *Escherichia coli* occurs in a similar orientation-dependent manner. For successful internalization, bacteria must be trapped by macrophages by one of their poles; otherwise, macrophages need to reorient the filaments engaged along their long axis in order to trap and engulf them (Möller et al., 2012). Once filamentous bacteria are properly engaged for phagocytosis, their uptake progresses at a similar speed as for bacillary bacteria (Möller et al., 2012). Therefore, the phagocytic uptake occurs gradually and its duration lasts according to the length of the target. The effect of this gradual internalization on phagocytic cup remodeling and phagosomal maturation is unknown.

Several bacterial species switch from bacillary to filamentous morphology to endure stressful conditions, including sublethal doses of antibiotics, predation from protists, and immune responses (Justice et al., 2008). Thus, filamentation may favor bacterial escape from phagocytosis stochastically, by reducing the chances of phagocytic cells encountering their poles (Möller et al., 2012). Using paraformaldehyde-killed filamentous *Legionella pneumophila* as a target, we present evidence that the phagocytosis of filamentous bacteria deviates from the canonical phagocytic pathway that has been delineated with spheroidal targets. In contrast to what has been previously reported, our data provide evidence that the events associated with phagosomal maturation can occur at the level of the phagocytic cup, before its sealing and scission from the plasma membrane. Filament internalization occurs through a long-lasting, tubular phagocytic cup that fuses with endosomal and lysosomal compartments. Nevertheless, complete internalization of the filament and phagosome formation are required for these tubular phagocytic cups to develop degradative properties. Remarkably, this morphology-dependent alteration in the timing of phagocytosis enhances the ability of *L. pneumophila* to replicate inside macrophages in a length-dependent manner.

Results

Filamentous bacteria are gradually phagocytosed into a tubular phagocytic cup

To investigate how filamentous morphology impacts the morphogenesis and remodeling of the phagocytic cup, we followed the phagocytosis of IgG-opsonized filamentous *L. pneumophila* (*Lp*), obtained as previously described in Prashar et al. (2012) (see Materials and methods). Because *Lp* is an intracellular pathogen in phagocytic cells (Horwitz and Silverstein, 1980), filamentous *Lp* were killed with PFA (referred to as FBTs to denote filamentous bacterial targets) before being presented as targets to RAW 264.7 macrophages (RAW cells) to avoid the interference of bacterial toxins with phagocytosis. Time-lapse imaging of RAW cells expressing the plasma membrane probe GPI-GFP (Nichols et al., 2001) showed that FBTs were gradually engulfed by pseudopodia that extended along the long axis of the targets, forming a tubular phagocytic protuberance (Fig. 1 A and Video 1). Scanning electron microscopy (Fig. 1 B) and 3D rendering of confocal planes (Video 2) clearly depicted this tubular structure. The portion of the filament entrapped by the extending protuberance, distinguishable by differential immunostaining, was contained in a phagocytic cup, as delineated by the plasma membrane probes GPI-GFP (Fig. 1 C) and PM-GFP (Fig. S1 A; Teruel et al., 1999). The phagocytic cup followed the morphology of the target and appeared as a long, tubular plasma membrane invagination (referred to as T-PC for a tubular phagocytic cup) that extended from the phagocytic protuberance into the cellular body, eventually curving around the nucleus to accommodate the incoming FBT.

The T-PCs undergo similar remodeling as the phagocytic cups of small targets

The remodeling of phagocytic cups for large spherical particles (>3 µm) differs from those for small diameter targets, including bacillary bacteria (Lee et al., 2007; Tollis et al., 2010). To reach completion, the phagocytosis of large particles requires more extensive actin remodeling (Cox et al., 1999). This is accompanied by the mobilization of intracellular sources of membranes by focal exocytosis at the base of the phagocytic cups, controlled by downstream signaling mediated by class I phosphatidylinositol 3′-kinase (PI3K) activity at the phagocytic cup (Bajno et al., 2000; Braun et al., 2004; Cox et al., 1999). Therefore, we investigated if phagocytosis of FBTs was PI3K dependent. As previously shown, the pretreatment of RAW cells with the PI3K inhibitor Ly294002 (Ly) did not affect the binding of red blood cells (RBCs), but impeded their uptake (Fig. 1 D; Araki et al., 1996, 2003; Cox et al., 1999). Similar results were obtained with 8.3-µm beads (unpublished data). However, unlike for large spheroidal targets, inhibiting PI3K reduced FBT binding to RAW cells (Fig. 1 D), probably indicating a role for PI3K activity in the membrane–cytoskeleton remodeling needed for the reorientation of FBTs, which is necessary for the engagement of the bacterial poles for phagocytosis. Notably, despite the comparatively large magnitude of the phagocytic protrusions and phagocytic cup required to engulf FBTs, Ly294002 did not effect their internalization (Fig. 1 D). This suggests that filaments are sensed and internalized through mechanisms that correspond to the phagocytosis of small diameter particles. Indeed, unlike the phagocytosis of 8-µm beads where the focal exocytosis of endomembranes causes the loss of plasma membrane markers from the base of their phagocytic cups (Lee et al., 2007), this was not the case for T-PCs (Fig. 1 C, Fig. S1 A, and Video 2).

GPI-GFP from fully internalized FBTs (arrows) are indicated. (D) PI3K activity is not required for FBT internalization. Cells pretreated with 100 µM LY294002 (Ly) for 30 min were presented with opsonized RBCs or FBTs and phagocytosis allowed to proceed for 50 min in the presence of Ly. Cells were fixed, external particles were immunolabeled, and cells permeabilized to visualize internal particles. Attachment was enumerated for random fields. Efficiency of internalization was determined by assessing the proportion of internalized particles/total particles. Data shown are means ± SEM from three independent experiments. For binding efficiency, n = 150 RAW cells and for internalization efficiency, n = 100 RBCs or 30 FBTs in each experiment. Bars: (main panels) 5 µm; (magnifications) 2.5 µm.

Actin remodeling regulates T-PC elongation and particle internalization

Actin remodeling plays an important role in sustaining the capture and promoting the internalization of targets by phagocytosis. Upon Fcγ receptor activation, downstream signaling leads to a strong F-actin accumulation around the target and in the pseudopodia within the first minutes of the process (Scott et al., 2005). As phagocytosis progresses, F-actin is removed from the base of the phagocytic cup and only remains in the extending pseudopodia (Botelho et al., 2004). This reduces cortical tension, facilitating the invagination of the plasma membrane at the cup beneath the targets, and leads to their uptake (Raucher et al., 2000). Similarly, as the uptake of the FBTs progressed, F-actin disappeared from the base of the T-PCs but accumulated around the filaments in the advancing end of the phagocytic protuberance in a "jacket"-like structure, which, although dynamic, persisted until the FBTs were fully internalized (Fig. 2 A and Video 3). Stabilizing F-actin with jasplakinolide stalled the elongation of the T-PCs and the uptake of FBTs (Fig. 2, B and C), altogether indicating actin treadmilling is probably required for sustaining the actin jackets and for the extension of the phagocytic protuberance over the FBTs.

The biphasic distribution of actin in the phagocytic cups is correlated with changes in the content of phosphatidylinositol 4,5-bisphosphate ($PI(4,5)P_2$) in the plasma membrane engaged in phagocytosis (Botelho et al., 2000, 2004). This phospholipid plays a key role in promoting actin assembly and remodeling at the plasma membrane, and its dynamics at the phagocytic cup of spheroid targets parallel that of actin (Botelho et al., 2000; Scott et al., 2005). Similar to the phagocytosis of beads, the disappearance of $PI(4,5)P_2$ from the base of the T-PCs (Fig. 2 D) and the concomitant appearance of diacylglycerol (Fig. 2 E), detected through the fluorescent probes PLCδ-PH-GFP (Stauffer et al., 1998) and PKC-C1δ–GFP (Botelho et al., 2000), respectively, suggested the hydrolysis of PI(4,5)P2 by the phospholipase Cγ (PLCγ; Botelho et al., 2000). Altogether, these data indicate that the T-PCs undergo similar actin remodeling as the phagocytic cups formed for spheroidal targets.

The T-PCs undergo phagosomal maturation independently of phagosomal sealing

Immediately after the phagocytic cup seals around a spheroidal target, the newly formed phagosome undergoes a maturation process through sequential fusion events with endosomal compartments. Given the long duration required for FBT internalization, we sought to investigate if they interacted/fused with endocytic compartments. Interestingly, as early as 5 min after the attachment of FBTs to RAW cells, the base of the T-PCs, which had already lost F-actin accumulation, recruited the early endosomal markers EEA1 (Fig. 3 A) and 2FYVE-GFP (Fig. 3 B), a chimera fluorescent probe that binds phosphatidylinositol 3-phosphate (PI(3)P; Lawe et al., 2000; Mills et al., 1998). Both of these are key components of early endosomal membranes that promote homotypic fusion and their subsequent maturation into late endosomes. This suggested that the T-PCs were likely undergoing a similar maturation process as has been described for phagosomes containing spheroidal targets. Indeed, after priming the actin-free tip of the T-PCs, early endosomal markers disappeared and the late endosomal and lysosomal makers Rab7 and lysosomal-associated membrane protein 1 (LAMP1) were both recruited to the T-PCs (Fig. 3, C–E). To investigate if active lysosomes fused with the T-PCs before phagosomal sealing, we used DQ-ovalbumin (DQ-ova), a self-quenched protease substrate that is converted into fluorescent peptides by lysosomal proteases (Björck et al., 2008), to label these organelles. Fig. 3 (F and G) shows that T-PCs formed in DQ-ova–loaded RAW cells retained fluorescent peptides in their lumen, indicating that metabolically labeled lysosomes fused and discharged their contents in the T-PCs. Taken together, these results suggest that T-PCs undergo changes corresponding to the phagosomal maturation process before their sealing.

The T-PCs fail to develop hydrolytic capacity

As phagosomes mature, they acidify and acquire hydrolases that degrade their cargo. Considering that T-PCs fused with lysosomes, we next assessed if they became hydrolytic. To this end, we presented RAW cells with FBTs cross-linked with DQ-ova and followed the development of fluorescence during phagocytosis. Although fully internalized FBTs fluoresced over time, which correlated well with bacterial degradation, suggesting lysosomal activity (Fig. 4 B, and Videos 4 and 5), partially internalized FBTs showed no DQ-ova fluorescence (Fig. 4 A). These results indicated that even though there was an extensive fusion with lysosomes as shown above (Fig. 3), the T-PCs failed to develop hydrolytic capacity. Aiming to reconcile both observations, we assessed whether the T-PCs were acidic and if they contained lysosomal hydrolases. The acidotropic dye LysoSensor failed to label the T-PCs, whereas it strongly fluoresced in phagosomes (Fig. 4, C and D), indicating that T-PCs were not acidic. This is in agreement with the fact that although GFP fluorescence is quenched by acidic pH (Elsliger et al., 1999), GPI-GFP, which faces the lumen of the T-PCs, retained its fluorescence until FBTs were completely internalized (Fig. 1 C). Phagosomal acidification is accomplished by the V-ATPase proton pump, which is recruited to these compartments along the maturation process (Lukacs et al., 1991; Sun-Wada et al., 2009). The voa3 subunit of V-ATPase (Saw et al., 2011) was strongly recruited to the T-PCs (Fig. 4 E), indicating that the lack of T-PC acidification was not due to a deficiency in proton pump recruitment. However, despite their fusion with lysosomes, T-PCs were mainly devoid of lysosomal hydrolase cathepsin-D. This enzyme was otherwise detectable in FBT-containing phagosomes by 1 h, showing a strong accumulation by 6 h (Fig. 4 F).

Although T-PCs are open structures, Figs. 1 C and 3 F suggest the presence of diffusion barriers that impede the free movement of antibodies and DQ-ova fluorescence peptides in and out, from the lumen of the T-PC. Therefore, assuming that the V-ATPase is functional and that lysosomes were fusing with the T-PCs, we reasoned that the lack of the hydrolytic capacity of the T-PCs could be due to protons and small lysosomal hydrolases leaking out into the extracellular milieu. To investigate this, we next assessed the existence of putative diffusion barriers and determined their molecular weight cut-off. Late endosomes

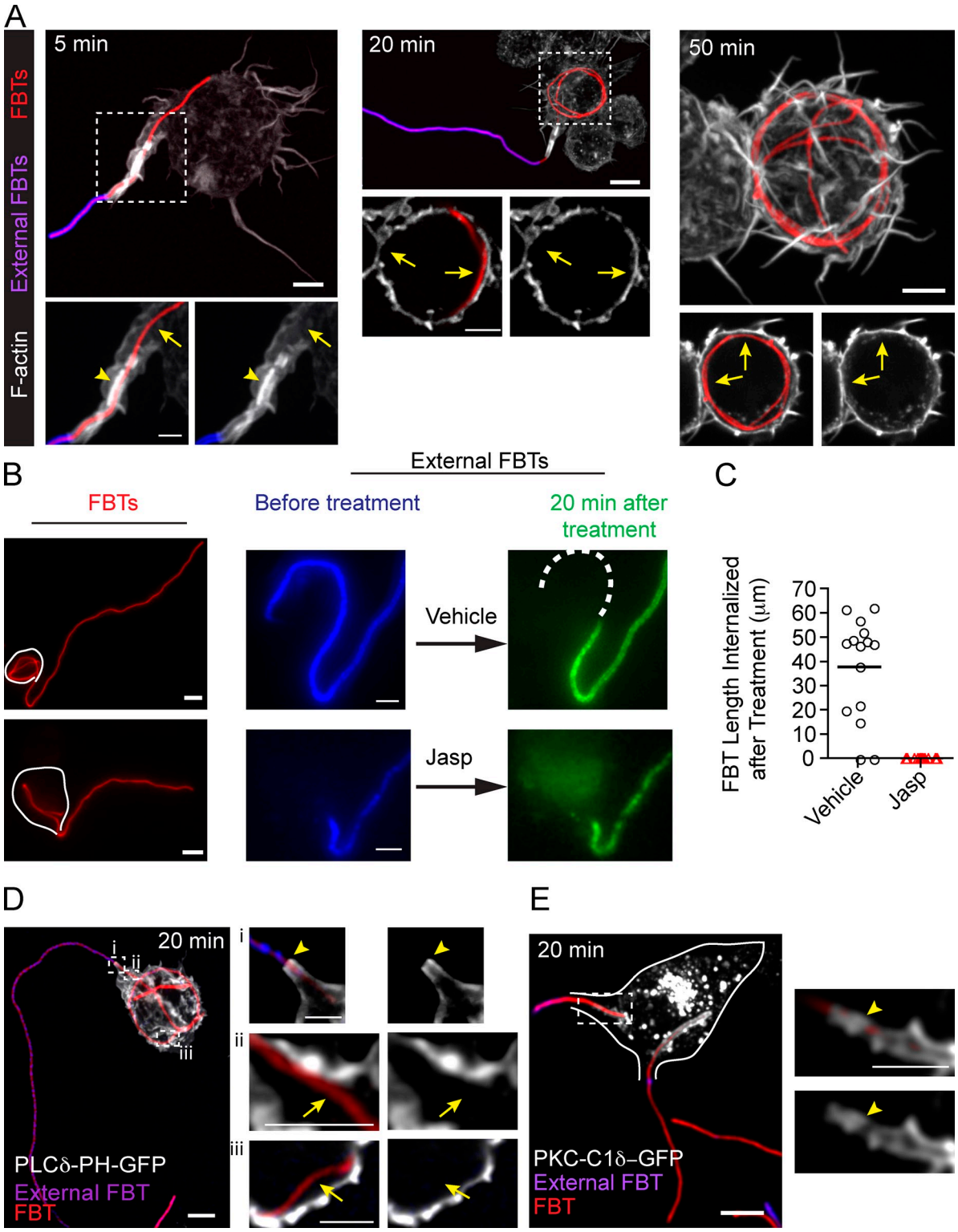

Figure 2. **T-PC elongation requires actin turnover.** (A) F-actin was enriched in the T-PC (arrowhead) forming the actin jacket but disappeared as the filament continued to get internalized (arrows). Cells were fixed at indicated times after FBT phagocytosis, external FBTs were immunolabeled (pink), and F-actin was stained using Phallodin 488 (white). (B) After 20 min of phagocytosis, external FBTs were immunolabeled (blue) in the cold. Phagocytosis was then allowed to progress in the presence of jasplakinolide (jasp, 20 min). External FBTs were immunolabeled (green) and cells were fixed. Dashed line in the panels to the right indicates the FBT length internalized during the treatment. (C) Lengths of FBTs internalized after the treatment in B. Data shown are FBT lengths from a representative experiment out of three repeats. Lines indicated the means. For the experiment shown, $n = 15$. (D) $PI(4,5)P_2$ disappeared as FBTs were internalized. Phagocytosis of FBT by cell expressing PLCδ-PH-GFP (white). Cells were fixed after 20 min of phagocytosis and external FBTs were immunolabeled (pink). Right: magnified single planes from framed regions. The presence of $PI(4,5)P_2$ at the T-PCs (arrowheads) and its loss as FBTs are internalized (arrows) are indicated. (E) Diacylglycerol appeared as FBTs were internalized. Phagocytosis of FBT by cell expressing PKC-C1δ–GFP (white). External FBTs are shown in pink. Right: magnified single planes from framed regions. White lines delineate the cell boundary. Bars: (main panels) 5 μm; (magnifications) 2.5 μm.

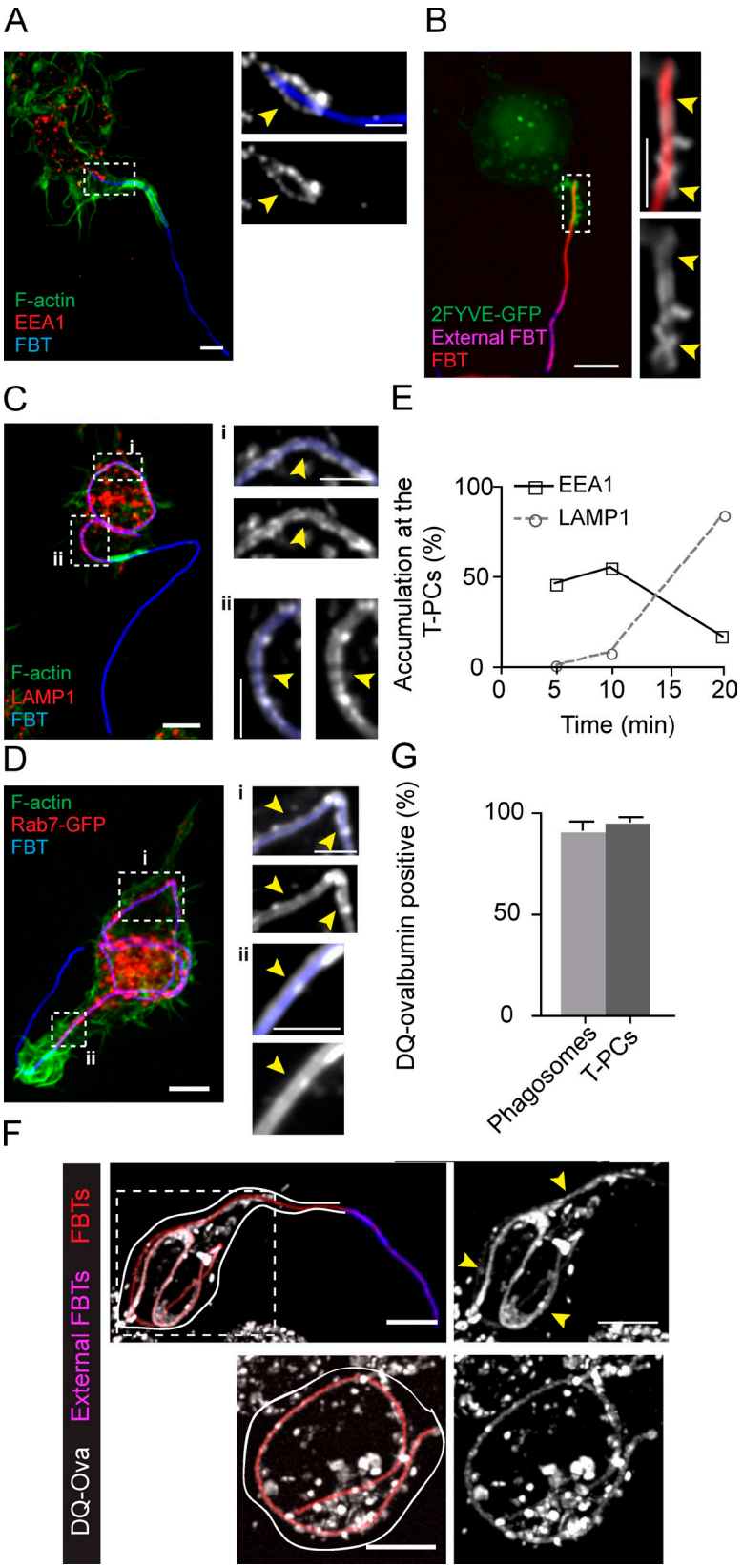

Figure 3. **The T-PCs fuse with endosomal and lysosomal compartments.** (A) EEA1 and F-actin distribution in cells after 5 min of phagocytosis. Right: magnified single planes from framed regions. Arrowheads indicate EEA1 recruitment (white) around FBT where F-actin (green) is lost from the base of the T-PC. (B) 2FYVE-GFP accumulation around FBT after 5 min of phagocytosis. Right: magnified single planes from framed regions. Arrowheads indicate the accumulation of 2FYVE (white) around internalized FBT segments. External FBT sections are shown in pink. (C) LAMP1 (red) localization around internalized FBTs, where actin (green) is lost from the base of the T-PC. Right: magnified single planes from framed regions. Arrowheads indicate LAMP1 accumulation (white). (D) Rab7-GFP (red) accumulation around internal FBT segments. FBTs were added to cells expressing Rab7-GFP, cells were fixed after 20 min of phagocytosis, permeabilized, and actin was stained with phallodin (green). Right: magnified single planes from framed regions. Arrowheads indicate Rab7 accumulation (white). (E) Accumulation of EEA1 or LAMP1 around internal FBT sections over time. Cells were immunolabeled for both EEA1 and LAMP1 and partially internalized FBTs were scored for the accumulation of these markers. Data shown are percentages from a representative experiment out of three repeats. For the data shown, $n = 80$ at each time point. Note: none of the FBTs were positive for both markers. (F) Lysosomes fuse with T-PCs. Cells preloaded with DQ-ova were allowed to ingest FBTs for 20 min. Cells were fixed and external FBTs were immunolabeled (pink). Top: DQ-ova accumulation (white) around internal parts of FBT (arrowheads). Right: higher magnification of the framed regions. Bottom: DQ-ova accumulation around fully internalized FBT (arrowheads). Solid lines delineate cell boundaries. (G) The number of partially and fully internalized FBTs surrounded by DQ-ova from (F). Data shown are means ± SEM from three independent experiments. At least 50 FBTs were analyzed in each case. Bars: (main panels) 5 µm; (magnifications) 2.5 µm.

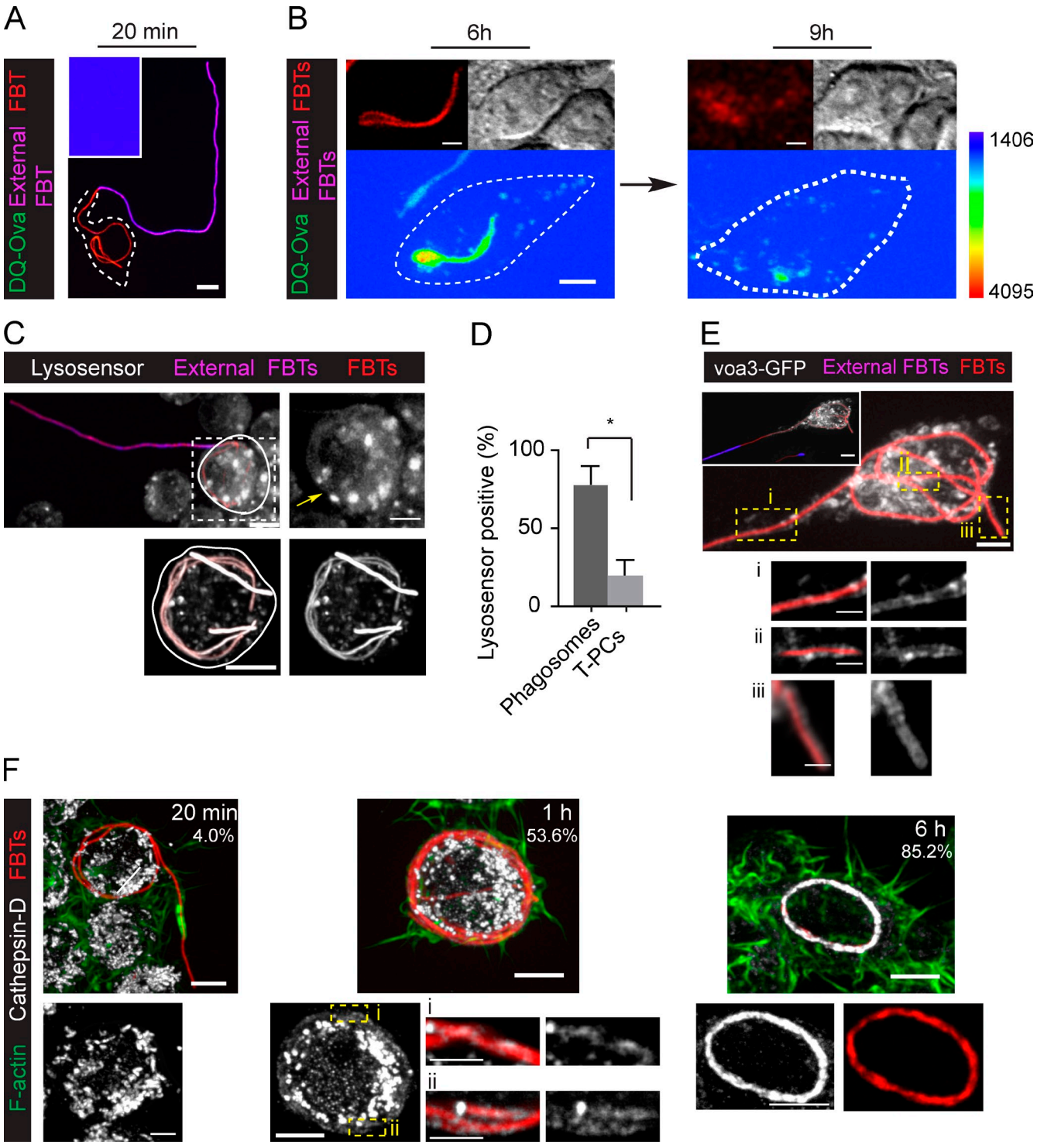

Figure 4. **T-PCs are not hydrolytic compartments.** (A and B) RAW cells ingesting FBTs cross-linked with DQ-ova. (A) Partially internalized FBT after 20 min of phagocytosis. Inset shows the lack of DQ-ova fluorescence. (B) Images from live-cell video microscopy showing fully internalized FBT undergoing degradation as detected by DQ-ova fluorescence (image acquisition using EM-CCD camera; Hamamatsu Photonics). External FBTs were labeled in the cold before imaging (not depicted). (C) Top: LysoSensor fails to label partially internalized FBTs (arrow), but accumulates around fully internalized FBTs (bottom panels). 20 min after phagocytosis external FBTs were immunolabeled in the cold (pink). Lysosensor was added (2 min) and cells moved to precooled microscope stage. White lines indicate cell boundaries. (D) The number of partially and fully internalized FBTs positive for lysosensor from C. Data shown are means ± SEM from three independent experiments; $n = 25$. (E) V-ATPase proton pumps surround the T-PCs. Phagocytosis of FBTs by cells expressing voa3-GFP (white) subunit of V-ATPase. Cells were fixed after 20 min of phagocytosis and external FBTs were labeled (pink, inset). Bottom panels: magnified single planes from framed regions. (F) Cathepsin-D in cells internalizing FBTs. Cells were fixed at indicated times, F-actin was stained (green), and cathepsin-D was immunolabeled (white). The percentage of FBTs positive for cathepsin-D at each time point is indicated. Data shown are means from two independent experiments. Atleast 25 FBTs were assessed in each case. Bars: (main panels) 5 µm; (magnifications) 2.5 µm.

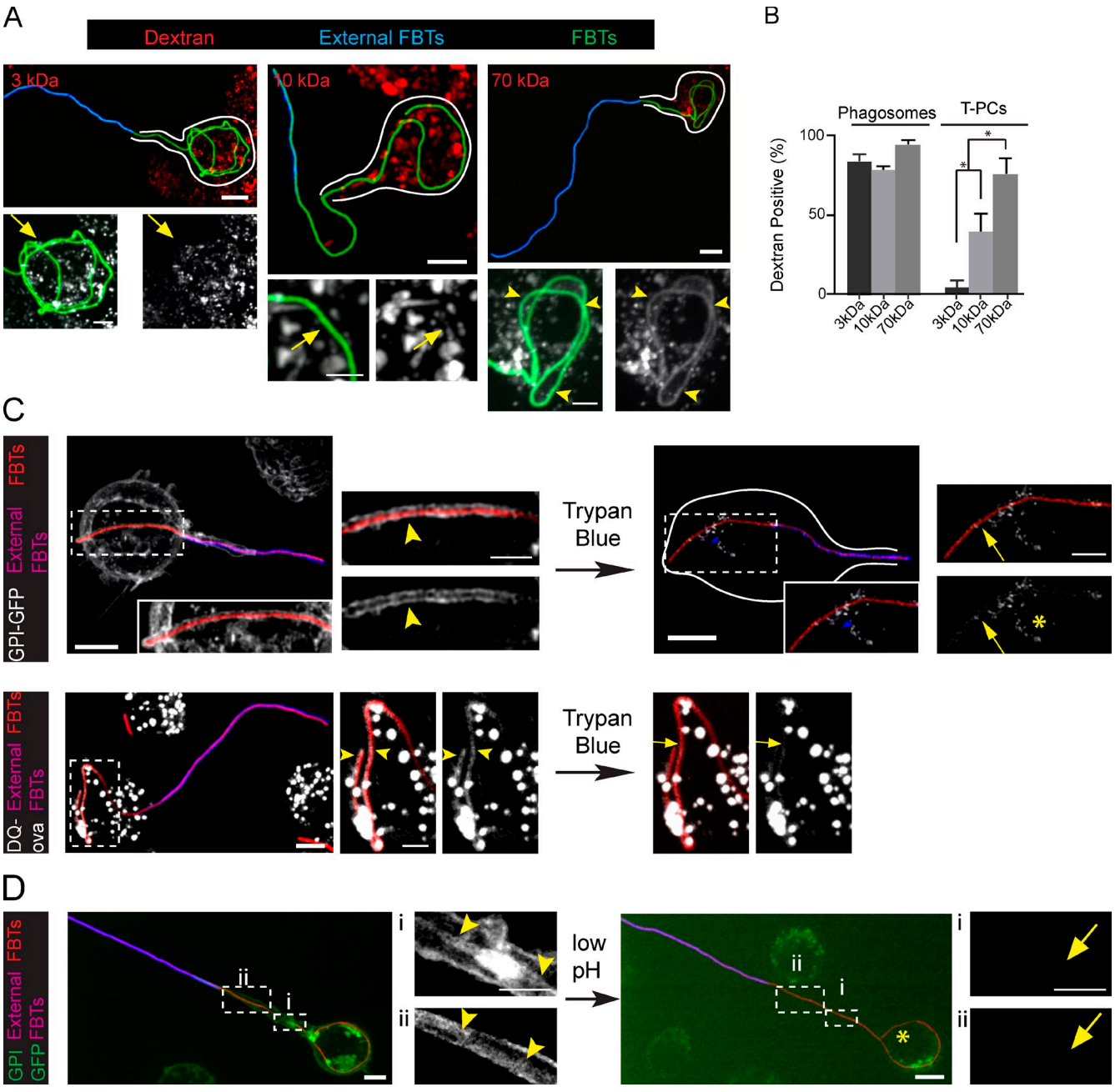

Figure 5. **Low molecular weight solutes permeate across the T-PCs.** (A) RAW cells preloaded with 3-, 10-, and 70-kD rhodamine dextrans with pulse and chase were allowed to ingest GFP-FBTs for 20 min and external FBTs were immunolabeled (blue). Top: partially internalized FBTs. White lines indicate cell boundaries. Bottom: higher magnifications of internal segments of FBTs. Dextrans are shown in white. 70-kD dextran accumulated around internal portions of FBTs (arrowheads), while 3-kD and 10-kD dextrans were absent (arrows). (B) The number of partially and fully internalized dextran-positive FBTs from A. Data shown are means ± SEM from three independent experiments; $n = 50$. (C) Trypan blue leaks into the T-PCs and quenches GPI-GFP (white) fluorescence from the T-PC membrane (top panels) and DQ-ova (white) from T-PC lumen (bottom panels). After 20 min of FBT phagocytosis by cells stably expressing GPI-GFP, external FBTs were labeled in the cold. Cells were moved to a precooled microscope stage and trypan blue was added to the extracellular media. Left: GPI-GFP– and DQ-ova–positive T-PCs (arrowheads). Right: GFP from T-PCs is quenched by trypan blue (arrows). Endosomes that were inaccessible to trypan blue were not quenched (asterisk). (D) T-PCs are permeable to protons. 20 min after phagocytosis of FBTs in GPI-GFP–expressing cells, external FBTs were labeled in the cold (pink). Cells were moved to a precooled microscope stage and extracellular pH was reduced to 4.0. Right: arrowheads indicate the T-PC containing GPI-GFP (white). Left: quenching of GFP from the T-PC (arrows) after reducing extracellular pH. Asterisk denotes endosomes not affected by the treatment. Bars: (main panels) 5 µm; (magnifications) 2.5 µm.

and lysosomes were preloaded with fluorescent dextrans of different molecular weights by fluid-phase uptake as described elsewhere (Harrison et al., 2003). Macrophages were then exposed to FBTs and the ability of T-PCs to retain the dyes after lysosomal fusion was assessed. All the dextrans used accumulated in phagosomes containing FBTs (Fig. S2). However, whereas 70 kD was retained in the T-PCs, 3-kD dextrans completely leaked out and 10 kD was retained with a lower efficiency (Fig. 5, A and B). Next, we examined if the lumen of the T-PCs was accessible to small solutes from outside the cell. To this end, we

used the dye trypan blue (1 kD), which can quench green emission fluorescence (Hed, 1986; Vasselon et al., 1999). Externally applied trypan blue was able to quench fluorescence from GPI-GFP and DQ-ova derived peptides in the membrane and the lumen of the T-PCs, respectively (Fig. 5 C). To investigate if the T-PCs were permeable to protons, we took advantage of the fact that GFP fluorescence can also be quenched under low pH conditions (Elsliger et al., 1999). A brief pulse of acetate buffer (pH 4.0, 10 mM) caused the quenching of GPI-GFP fluorescence from the T-PCs (Fig. 5 D). Altogether, these results indicate that the diffusional barriers at the T-PCs allowed protons and hydrolases like cathepsin-D, with mature forms of 14 and 32 kD (Reiser et al., 2010), to leak out, therefore hindering the degradative capacity of macrophages.

Actin jackets contribute to the diffusional barriers at the T-PCs

The actin jacket delimited the penetration of immunofluorescence antibodies into the T-PC lumen and defined the margins in the protuberance reachable by fluid-phase markers delivered through lysosomal fusion. Therefore, we decided to investigate if the actin jackets play a role in creating the diffusion barriers. RAW cells were allowed to form T-PCs for 20 min. Phagocytosis was then paused by incubating at 4°C to immunolabel the external portion of the FBTs, thus marking the extent of phagocytic uptake. The phagocytic process was resumed by incubating at 37°C in the presence of F-actin depolymerization agents. After these treatments, external filaments were immunolabeled again to assess the effect on the diffusional barriers. Depolymerization of F-actin disassembled the actin jackets (Fig. 6, A and B) but the protuberances, visualized by PM-GFP, were not affected (Fig. S3 B). While completely internalized FBTs were not labeled (unpublished data), the disappearance of the actin jackets allowed the second round of antibodies to penetrate in the T-PCs and label the previously inaccessible FBT segments (Fig. 6, A and B). However, the diffusion of antibodies into the T-PCs was not affected when cells were treated with jasplakinolide (Fig. 2 B and Fig. 8 D), indicating that the actin jacket is required for the formation of diffusion barriers at the T-PCs but actin treadmilling is not necessary to sustain them.

These diffusion barriers could be the consequence of constriction forces applied by the actin jacket on the FBTs. Previous reports indicate that the actin rings formed at the rim of phagocytic cups exert such kinds of forces over their targets. The action of these forces can be clearly visualized as the squeezing of flexible targets like RBCs captured in phagocytic cups (Araki et al., 2003; Swanson et al., 1999). To investigate if the T-PCs can apply constriction forces on the FBTs, we used PFA-killed filamentous *Salmonella typhimurium* as targets (S-FBTs). Although S-FBTs were shorter than *Legionella* FBTs, they were thicker and facilitated the detection of constrictions along them. Analysis of 160 bacteria in three independent experiments showed that 51 ± 3.9% of S-FBTs were squeezed at the sites enclosed by the actin jackets (Fig. 7 A and Video 6). Inhibiting actin polymerization and remodelling prevented the formation of actin jackets and consequently, the formation of these constrictions. However, myosin II activity was dispensable for these processes (Fig. 7 B).

Collectively, these results suggest that the diffusion barriers are mediated by the actin jackets closing the aperture of the T-PCs. We reasoned that the close contact between the T-PCs and the target could favor the formation and/or stabilization of molecular sieves between them. This could involve transmembrane receptors cross-linking ligands from the FBTs with the actin jacket in the T-PCs. To investigate this possibility, we stabilized actin jackets with jasplakinolide (Fig. 8 A) and assessed the permeability of the T-PCs after protease treatment to cleave this putative receptor-ligand sieve. As suggested by the trends in Fig. 8, treatment with either trypsin (21 kD; Anderson et al., 1981) or papain (23.4 kD; Mitchel et al., 1970) allowed DQ-ova in the T-PCs to leak out (Fig. 8, B and C) and externally applied antibodies to penetrate into the T-PCs (Fig. 8, D and E). Altogether, these results indicate that the diffusion barriers depended on molecular sieves, probably formed by receptor-ligand binding. Because both T-PC formation and diffusional barriers occurred in the absence of opsonins (Fig. S5), this suggests that nonopsoninc receptors could mediate this process. However, the receptors involved in the nonopsonic uptake of *Lp* are unknown (Khelef et al., 2001; Tachado et al., 2008).

Filamentous morphology allows *L. pneumophila* to evade phagosomal killing

Because T-PCs are long-lasting, nonhydrolytic compartments, we speculated that filamentous bacteria held inside them could have longer time to inject effectors and interfere with phagocytosis before being exposed to a lysosomal environment. To investigate this, we followed the fate of intracellular viable *Lp* in RAW macrophages. Effectors secreted through the type IV secretion system allow *Lp* to avoid phagosomal trafficking, converting its intracellular compartment into an ER-derived vacuole, the *Legionella*-containing vacuole (LCV; Isberg et al., 2009).

While a majority of WT Lp02 bacteria were targeted to LCVs, all of the type IV secretion system–deficient bacteria (Lp02 Δ*dotA*) were targeted to phagosomes (Fig. 9, A and B). Fig. 9 B shows tubular compartments decorated with KDEL and LAMP1 containing intracellular Lp02 and Lp02 Δ*dotA* filaments, respectively. In agreement with our hypothesis, the trend in Fig. 9 C suggests that longer Lp02 were more frequently found in LCVs than in phagosomes, whereas Lp02 Δ*dotA* were always in phagosomes regardless of their length.

We next investigated whether length could favor intracellular replication of *Lp*. Live-cell imaging of individual intracellular bacterial filaments over time revealed that not only did filamentous Lp02 form an LCV, they were also able to replicate (Video 7). In the course of 15 h, the filaments first elongated (Fig. 9 D), followed by fragmentation, and produced multiple bacillary progeny by binary fission that escaped the cell, in the same way as we reported for filamentous Lp02 inside cultured lung epithelial cells (Prashar et al., 2012). This is illustrated in Video 7 and in the time-lapse video microscopy sequence from Fig. 9 E. After analyzing Lp02 filaments over several movies from independent experiments, we found that 33.0 ± 2.6% of intracellular Lp02 filaments replicated, while a small proportion of Lp02 failed to replicate or were destroyed (Fig. 9 F and Video 8). As expected, no replication was detected in the case of Lp02 Δ*dotA* filaments

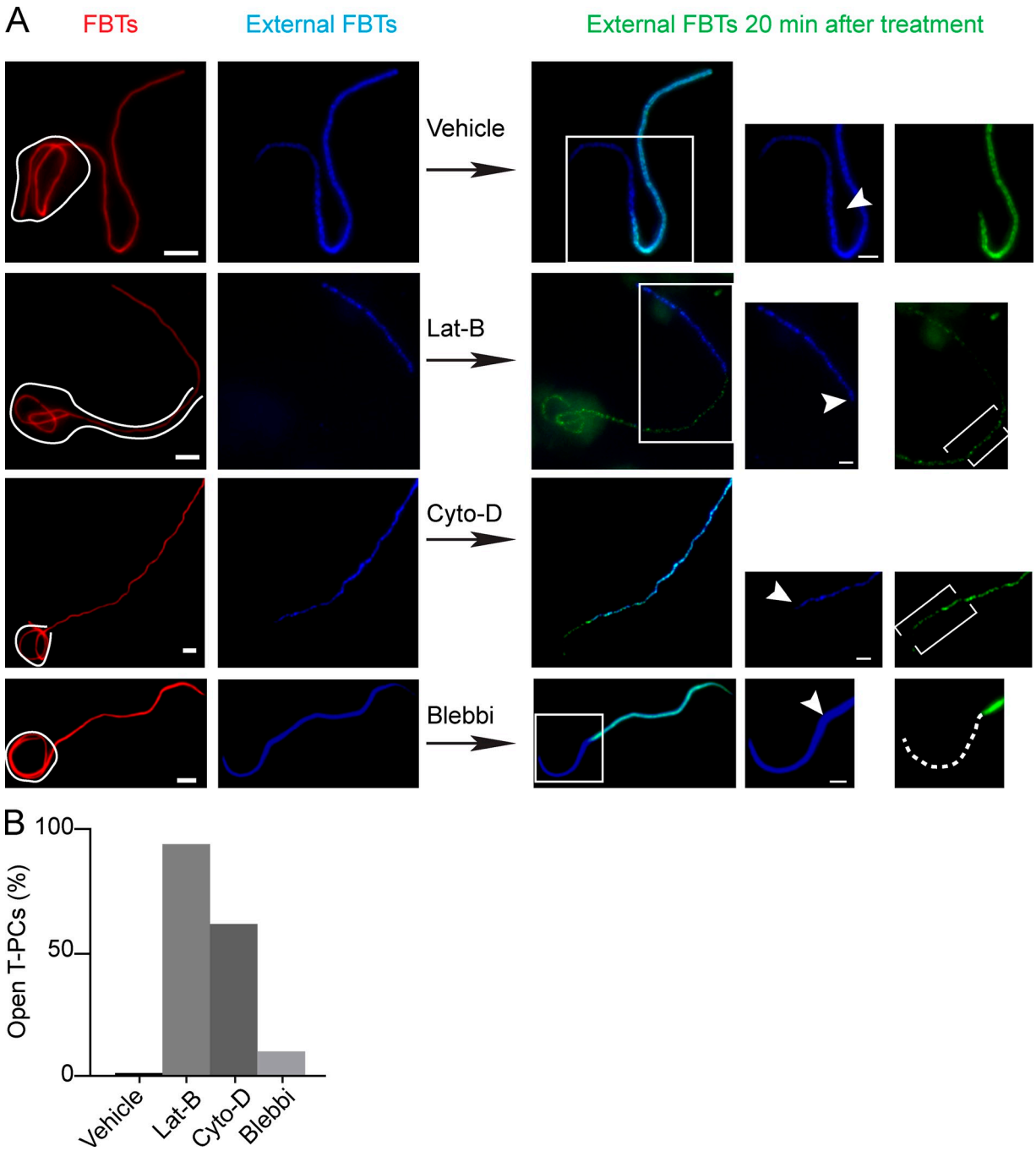

Figure 6. **Actin depolymerization disrupts the diffusion barriers at the T-PC.** Inhibiting actin dynamics removes the barrier that prevents antibodies from penetrating inside the T-PCs. 20 min after FBT phagocytosis, external segments of FBTs were immunolabeled in the cold (blue). Phagocytosis was allowed to proceed in the presence of latrunculin B (lat-B; 2 µM), cytochalasin D (cyto-D; 10 µM), blebbistatin (blebbi; 100 µM), or vehicle for 20 min and external FBTs were immunolabeled (green). (A) Inhibiting actin remodeling allowed the second round of antibody to penetrate inside the T-PCs (brackets) and label sections of FBTs previously inaccessible (green). Dashed lines in the panels to the right indicate FBT sections that remained inaccessible to the antibodies. (B) Number of T-PCs that lost the diffusion barrier from A. Data shown are percentages from a representative experiment from three repeats. For the experiment shown, $n = 50$. Bars: (main panels) 5 µm; (magnifications) 2.5 µm.

(Fig. 9 F). Assesment of the fate of intracellular Lp02 as a function of bacterial length showed a trend suggesting that the longest filaments were the ones that replicated more frequently (Fig. 9 G). This trend was in agreement with that from Fig. 9 C, which depicts the length-dependent trafficking of Lp02 to the LCV.

Collectively, these results indicate that in concert with effectors, filamentous morphology can aid *L. pneumophila* in evading macrophage killing and promoting intracellular replication.

Discussion

Here we present evidence that the phagocytosis of filamentous bacteria deviates from the canonical pathway delineated using spheroidal targets. This variation includes spatiotemporal alterations that affect the morphogenesis of the phagocytic cup and the maturation of the phagosome containing FBTs. Importantly, these changes along with effectors allowed *L. pneumophila*

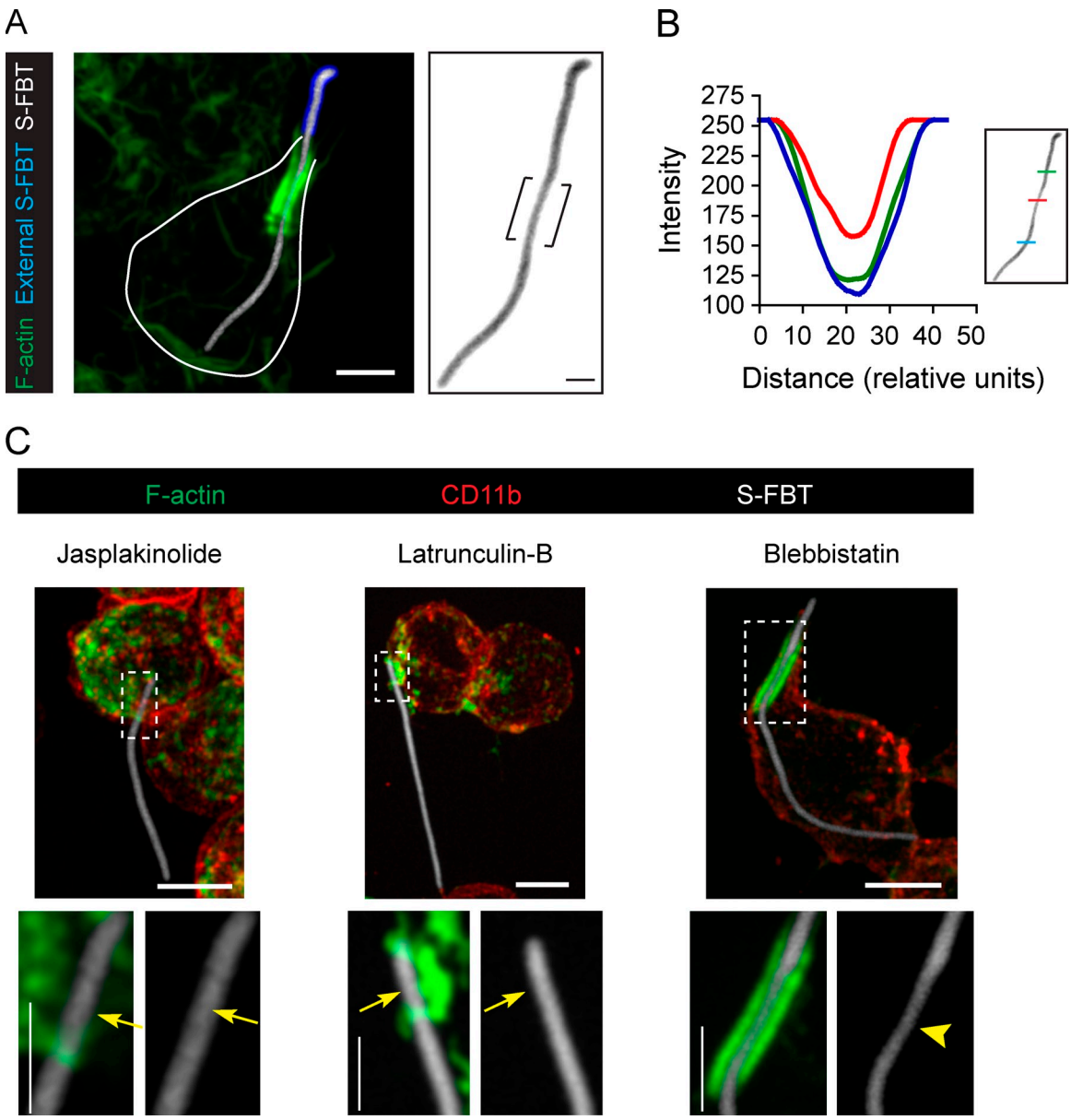

Figure 7. **Actin jackets constrict the *Salmonella*-FBTs.** (A) RAW cells were allowed to ingest RFP-*Salmonella*-FBTs (white) for 10 min. Cells were fixed, external sections of the S-FBTs were immunolabeled (blue), and F-actin was stained (green). Right: higher magnification of the S-FBT (inverted image), showing its constriction by the actin jacket (brackets). Solid line indicates the cell boundary. (B) Constriction of the S-FBT shown in A, as measured by the fluorescence intensity of the indicated regions along the filament. (C) S-FBTs (white) attachment to RAW cells was synchronized in the presence of blebbi (100 µM), jasp (1 µM), or lat-B (2 µM). Cells were fixed 10 min after the initial attachment, and cell membrane labeled with CD11b antibodies (red). F-actin is shown in green. Bottom: higher magnifications of framed regions. Arrowhead indicates S-FBT constriction due to the actin jacket and arrows point to the lack of T-PCs and the constriction of the S-FBTs. All micrographs shown are merged confocal planes (not deconvolved). Bars: (main panels) 5 µm; (magnifications) 2.5 µm.

to escape killing and replicate in macrophages in a length-dependent manner.

The key aspect of the above-described phenomena is that in comparison with the uptake of spheroidal particles, phagocytosis of FBTs required a long-lasting phagocytic cup. This distinguishing feature is determined by the way in which the FBT is captured and ingested. As previously described for *E. coli* (Möller et al., 2012), macrophages captured FBT by one of the bacterial poles and engulfed it along its long axis. We demonstrate that this process is mediated by pseudopodial protrusion that engulfs and simultaneously "threads" the filament into the cell. Similar to the extension of pseudopodia in the phagocytosis of spheroidal targets (Swanson and Baer, 1995), the elongation of the protrusion required actin turnover and thus could be inhibited by jasplakinolide. Although myosin II was dispensable for this process (Fig. S4 B), the involvement of other myosins, like myosin X (Cox et al., 2002), cannot be ruled out.

Despite the extensive actin remodeling and internalization of large amounts of plasma membrane to ingest FBTs, this process occurred independently of PI3K activity, resembling the uptake of small targets (Cox et al., 1999). This is likely because FBTs are internalized through their poles and hence, the aperture

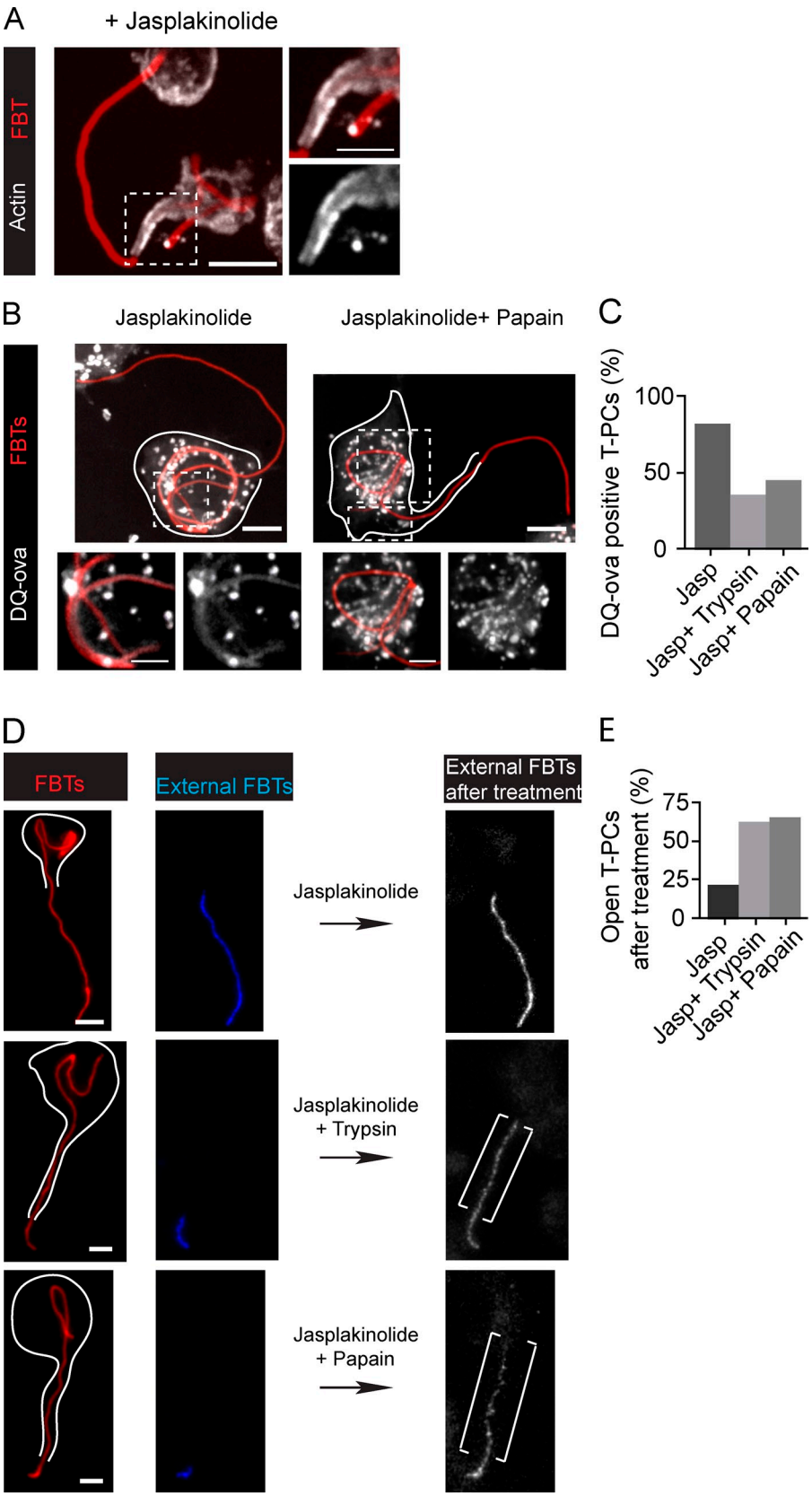

Figure 8. **Molecular sieves form the barriers at the T-PCs.** (A) After 20 min of phagocytosis, cells were treated with jasp and phagocytosis was allowed to continue (20 min). Actin was immunolabeled (white) to visualize jasp-stabilized actin jackets. Right: higher magnification of the framed region. (B) T-PCs become permeable to peptides derived from DQ-ova hydrolysis after treatment with externally applied proteases. 20 min after FBT phagocytosis in cells preloaded with DQ-ova, external FBT sections were labeled in the cold (not depicted). Cells were treated with jasp (20 min) followed by 20 min treatment with trypsin (not depicted) or papain (0.2 mg/ml) or left untreated. Bottom: magnified single planes from framed regions. (C) Number of T-PCs positive for DQ-ova from B. Data shown are percentages from a single experiment; $n = 30$. (D) T-PCs become permeable to externally applied antibodies after protease treatments. After 20 min of phagocytosis, external FBT sections were labeled, phagocytosis was allowed to proceed in the presence of jasp (20 min), and cells were then treated with trypsin or papain or left untreated for an additional 20 min. External sections of FBTs were labeled (white). Right: higher magnifications from framed regions. Brackets indicate antibody penetration after protease treatment. White lines indicate cell boundaries. (E) Number of T-PCs permeable to antibodies from D. Data shown are percentages from a single experiment, completed once ($n = 50$). All micrographs shown are merged z-planes (not deconvolved). Bars: (main panels) 5 µm; (magnifications) 2.5 µm.

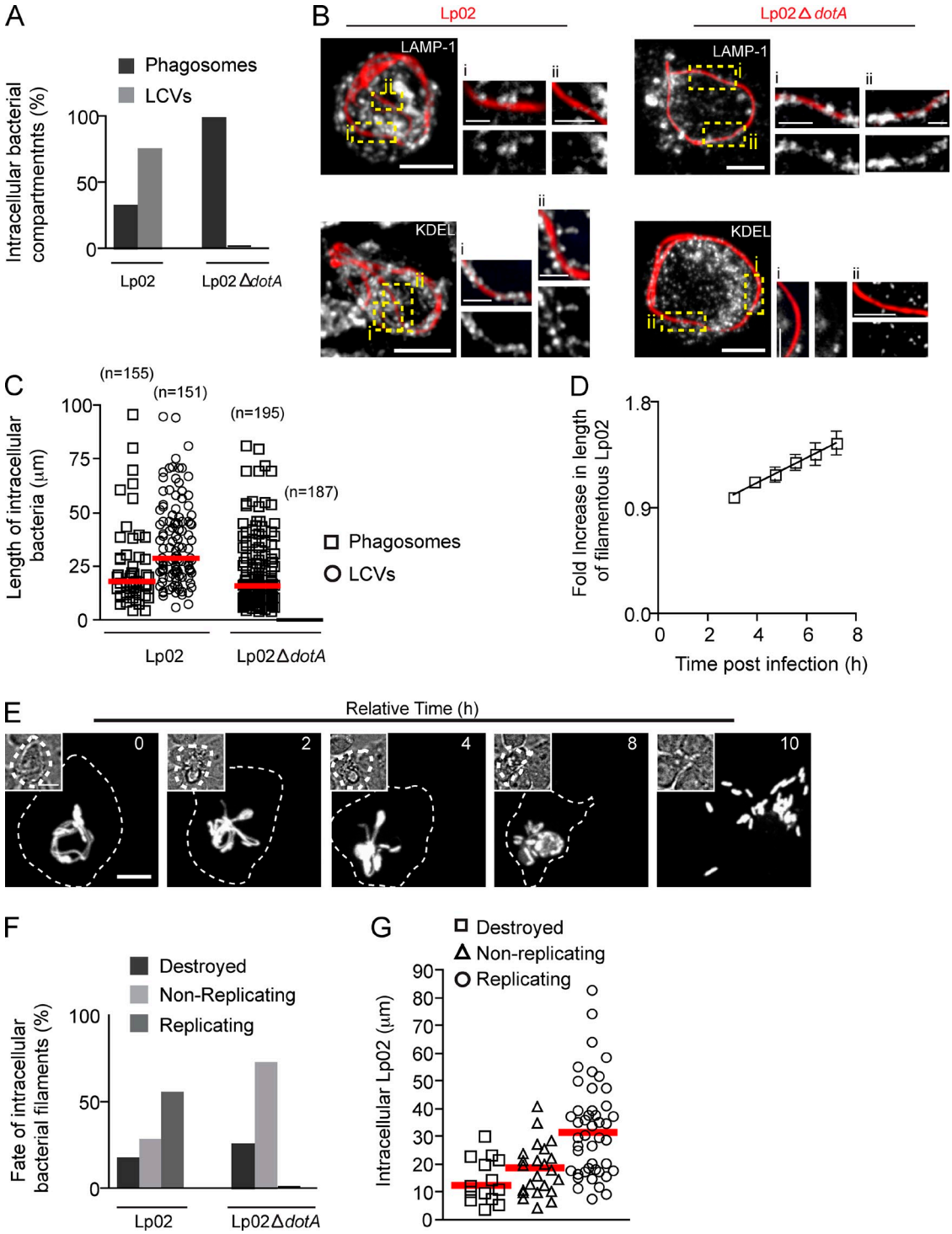

Figure 9. **Filamentous morphology contributes to *L. pneumophila* survival in macrophages.** (A) Number of intracellular RFP-Lp02 or RFP-Lp02-Δ*dotA* bacteria found in phagosomes and LCVs in macrophages infected for 9 h. Data shown are percentages from a representative experiment from two repeats. For the data shown, $n = 150$. (B) Representative images of intracellular RFP-Lp02 or RFP-Lp02-Δ*dotA* bacterial filaments from A. Right: magnified single planes from framed regions. (C) Length of intracellular bacteria and the associated compartment from A. Red lines indicate medians. (D–G) Live-cell video microscopy analysis. Images were acquired using an EM-CCD camera (Hamamatsu Photonics). RAW cells were allowed to internalize RFP-Lp02 or RFP-Lp02-Δ*dotA* for 5 h, gentamycin was added to the media, and time-lapse video was acquired for infected cells for an additional 15 h to follow the fate of intracellular bacteria. (D) Elongation of intracellular Lp02 filaments followed over time by time-lapse microscopy. Bacterial length was measured at indicated times using the software Volocity. Data shown are lengths from one representative experiment out of 3 repeats where 11 Lp02 filaments were analyzed. (E) Snapshots from time-lapse imaging of RAW cell infected with Lp02 showing the replication of filamentous Lp02 and production of bacillary progeny. Relative time is indicated on the top right corner and infected cell is delineated by dashed line. Insets show DIC images. (F) Infected cells were identified and followed over time to assess the fate of individual bacteria (destroyed, replicating, or nonreplicating). Data shown are percentages from a representative experiment out of two independent experiments. For the data shown, $n = 30$. (G) Length of intracellular Lp02 measured at the time the time-lapse acquisitions were started and their fate. Red lines indicate medians from three independent experiments. At least 15 intracellular Lp02 were analyzed in each case. Bars: (main panels) 5 μm; (magnifications) 2.5 μm.

of their phagocytic cups will be determined by the short axis of the filament, which is comparable to the size of small targets, including bacillary bacteria. Therefore, our results suggest that the aperture of the phagocytic cup could play a decisive role in how cells detect particle size.

F-actin strongly accumulated, forming an elongated jacket around FBTs at the most distal portion of the phagocytic protrusion. Formation of these jackets required actin treadmilling; however, the structure, once formed, was resistant to jasplakinolide treatment. We present evidence indicating that these actin jackets provided constriction forces, as was evident by the squeezing of the bacteria enclosed by these structures. Actin jackets are homologous to the actin furrow that constricts erythrocytes (Araki et al., 2003) or the concave neck of budded yeast during phagocytosis by *Dictyostelium* (Dieckmann et al., 2010; Swanson et al., 1999). Similar to these processes, T-PC–mediated constrictions were independent of myosin II. Nonetheless, other myosin motors, like myosin I, could be responsible for providing such contractile forces (Araki et al., 2003; Dieckmann et al., 2010; Nakada-Tsukui et al., 2009).

These actin jackets likely mediate the formation of a diffusion barrier at the T-PC. Our data suggest that protease-sensitive molecular sieves, probably formed by nonopsonic receptors cross-linking the FBTs with the T-PCs, could be responsible for these barriers. Presence of fences at the phagocytic cups for spherical targets has been suggested (Golebiewska et al., 2011). Nevertheless, further work is required to elucidate the mechanisms involved in the formation of diffusional barriers.

In the canonical pathway of phagocytosis, the remodeling of the phagocytic cup precedes and facilitates the scission of the nascent phagosome from the plasma membrane (Flannagan et al., 2012). The latter event is considered a *sine qua non* condition for the initiation of the maturation of the newly formed phagosome. However, notably, our results demonstrate that this scission from the membrane is not necessary for maturation, as T-PCs can undergo the same maturation steps as described for phagosomes in the canonical pathway. This crucial difference between the phagocytic cup of spheroidal and filamentous targets is most likely a consequence of the longer time required for the sealing of the T-PCs. The duration of the phagocytic cup stage during phagocytosis of FBTs could simply provide enough time for maturation to occur before the sealing of the cup. Indeed, the timings of the acquisition of phagosomal maturation markers by the T-PCs correspond well to those reported elsewhere for spheroid targets (Vieira et al., 2002).

Despite fusing with lysosomes and recruiting V-ATPases, the T-PCs failed to acidify and develop degradative properties. This was the consequence of the large molecular weight cut-off of the diffusion barriers at the phagocytic protrusion that allowed the leaking of small molecules into the milieu. Consequently, acidification and proteolytic activity was not detected in the T-PCs but was observed only after phagosomes were formed.

According to the established phagocytic pathway, acidification of the phagosome is necessary for its fusion with the endocytic compartments needed for phagosomal maturation. This concept is based on results from treatments where both the endosomes and the phagosomes were neutralized, making it difficult to distinguish if one or both of the two compartments need to be acidified for fusion to occur (Flannagan et al., 2012; Vieira et al., 2002). Our results show that the T-PCs, although neutral, can fuse with late endosomes and lysosomes, indicating that an acidic pH of endosomal compartments is likely the one required for this fusion and not necessarily that of the phagosomes.

Our data show that the aforementioned phenomena, along with the extended time required for phagosome sealing, has profound implications for the microbicidal capacity of macrophages. Filamentous *Lp* can escape phagosomal killing and replicate inside macrophages in a length-dependent manner. This suggests that the long residence time in the T-PCs could facilitate filamentous *Lp* survival by allowing the bacteria to maximize the delivery of effectors into the host cells before phagosomal sealing. This would allow them to modify their intracellular compartment to favor survival and replication. Of note, a similar mechanism could potentially account for the inhibition of phagocytosis reported for filamentous uropathogenic *E. coli* (UPEC; Horvath et al., 2011). The uptake of pathogens by macrophages and their subsequent degradation in the phagolysosomes constitutes an important component of the innate immune system (Flannagan et al., 2009). Filamentation has been observed for other pathogens in response to antibiotics (Chen et al., 2005; Comber et al., 1977; Davis et al., 1997; Nakao et al., 1981; Ryan and Monsey, 1981), and the long-lasting T-PCs could allow for effector secretion to stall and avoid phagocytosis as shown for filamentous UPEC (Horvath et al., 2011) or development of an intracellular replicative niche.

In summary, our results demonstrate that key aspects regarding the identity and remodeling of the phagocytic cup and the timing of phagosomal maturation are in fact conditioned by the morphology of the target.

Materials and methods

Reagents, antibodies, and DNA constructs

FBS and DMEM were obtained from Wisent. Sheep RBCs and rabbit anti–sheep antibodies were from MP Biomedicals. Alexa Fluor–conjugated secondary antibodies and phalloidin, LysoSensor green, tetramethylrhodamine dextrans, carbodiimide cross-linker, and DQ-ovalbumin were from Life Technologies. Anti-EEA1 antibody was from Santa Cruz Biotechnology, Inc., and anti-LAMP1 was from Developmental Studies Hybridoma Bank. The anti–phospho-Myosin II-LC2 (ser19) and anti–cathepsin-D antibodies were from Cell Signaling Technology, and the anti-KDEL antibody was from Enzo Life Sciences. Cytochalasin D and jasplakinolide were from EMD Millipore. Reagents for electron microscopy, latrunculin B and blebbistatin, were from Sigma-Aldrich.

The mammalian expression vector PM-GFP encodes the myristoylation/palmitoylation sequence from Lyn fused to GFP in pcDNA3 vector (Teruel et al., 1999). Rab7-GFP encodes WT Rab7 cloned into pEGFP-C1 vector (Bucci et al., 2000); 2FYVE-GFP encodes two tandem copies of FYVE of EEA1 fused to GFP (Gillooly et al., 2000). GFP-PLCδ-PH encodes the PH domain of PLCδ fused to GFP in vector C1 (Takara Bio Inc.) and GFP-PKC-C1δ encodes the C1 domain of PKCδ fused to GFP in vector N2 (Takara Bio Inc.; Stauffer et al., 1998; Botelho et al., 2004). Lentivirus-mediated expression vector EmGFP-voa3 encodes the voa3 subunit of V-ATPase fused with emerald GFP in pLVX-IRES-blast, and was used for transient transfections (Saw et al., 2011).

Cell culture and transfections

RAW264.7 cells were provided by R. Harrison (University of Toronto Scarborough, Toronto, Canada) and RAW264.7 cells stably transfected with GPI-GFP, a construct that consists of GFP anchored to glycosyl phosphatidylinositol (GPI; Nichols et al., 2001) and GFP-actin, a construct encoding

human brain β-actin fused to eGFP subcloned in pEF6/Myc-HisA vector under EF1-a promoter as described in Scott et al. (2005), were provided by S. Grinstein (Hospital for Sick Children, Toronto, Canada). Cells were cultured in DMEM with 10% heat-inactivated FBS at 37°C/5% CO_2. Transfections were performed using FuGENE HD (Roche) according to the manufacturer's instructions and cells were used after overnight expression of the plasmids.

Preparation of filamentous bacterial targets

Cultures enriched in filamentous *L. pneumophila* were obtained as described elsewhere (Prashar et al., 2012). In brief, bacteria from frozen glycerol stocks were streaked onto buffered charcoal-yeast extract (BCYE) agar and grown at 37°C and 5% CO_2. Colonies from 3–4-day-old plates were harvested and cultured for 24 h at 37°C in buffered yeast extract (BYE) media under low agitation (100 rpm). These precultures were subcultured at OD_{600} of 0.05 to get post-exponential growth phase bacteria with an OD_{600} of 3.5–4.0 (Molofsky et al., 2005). Next, cells were fixed in 4% PFA under slow agitation to obtain filamentous bacterial targets (FBTs). Growth in these conditions yielded bacillary and filamentous bacteria, with the latter ranging from 5 µm to >100 µm. For analyzing the here reported phagocytic uptake for filaments, bacteria longer than 5 µm were considered as filamentous targets. *L. pneumophila* strain Lp02, a streptomycin-resistant thymidine auxotroph derived from Lp01 strain (Berger and Isberg, 1993), was used in this study. All fluorescent strains and mutants were made in the Lp02 background.

RFP-Lp02 and GFP-Lp02 strains used were described previously (Duncan et al., 2011; Prashar et al., 2012). To obtain GFP-Lp02, the Lp02 *icmR* promoter was cloned upstream of the GFP gene into promoterless pBH6119 plasmid (Hammer and Swanson, 1999), and the resultant plasmid was used to transform Lp02. Lp02 Δ*dotA* strain was provided by A. Ensminger (University of Toronto, Toronto, Canada; Rao et al., 2013). It is a spontaneous Lp02 *dotA* mutant that is deficient in Dot/Icm translocation and was originally isolated based on its resistance to thymineless death in macrophages (Berger and Isberg, 1993). To obtain RFP-Lp02 and RFP-Lp02 Δ*dotA*, bacteria were transformed with the KB288 (magA/mCherry/pBH6119) plasmid, provided by A. Brassinga (University of Manitoba, Winnipeg, Canada). As described in Brassinga et al. (2010), the KB288 plasmid was generated by cloning *mCherry* from pmCherry plasmid into pBH6119 plasmid containing the Lp02 magA promoter.

To obtain *Salmonella typhimurium* filaments, RFP-expressing bacteria were used. The bacteria expressed mRFP protein under the promoter for the ribosomal protein RpsM (Birmingham et al., 2006). Bacteria were cultured overnight in LB and then sub-cultured for an additional 4 h. 0.5 µg/ml of ciprofloxacin was added to the cultures and bacteria were grown for an additional 6 h (Marathe et al., 2013). Bacteria were then killed with 4% PFA to get *Salmonella* filamentous bacterial targets (S-FBTs).

Preparation of DQ-ova–coated FBTs

FBTs were coated with DQ-ova as described previously (VanderVen et al., 2010; Yates and Russell, 2008). In brief, 10^9 filaments were resuspended in 1× PBS with 25 mg/ml carbodiimide cross-linker and agitated for 15 min. Excess carbodiimide was removed by three washes in 1 ml of 0.1 M sodium borate, pH 8.0 (coupling buffer). FBTs were resuspended in 500 µl of coupling buffer containing 1.0 mg DQ-ova and 40 µg of anti-Lp1 antibody for 12 h. Coated FBTs were washed three times with 250 mM glycine in PBS, pH 7.2 (quench buffer) by vortexing and centrifugation at 3,000 *g* for 5 min. FBTs were then washed three times with PBS before use in a phagocytic assay.

Phagocytosis assays and phagosome labeling

FBTs were opsonized with 0.1 mg/ml anti-Lp1 antibody for 1 h at RT. Unless stated otherwise, all phagocytosis assays were performed using PFA-fixed, IgG-opsonized RFP-Lp02 as FBTs. RAW (4×10^5) cells growing on glass coverslips were precooled at 15°C for 5 min and IgG-opsonized FBTs were then added (1 cell:50 FBTs). Unless specified otherwise, attachment was synchronized by spinning the FBTs onto the cells at 300 *g* for 5 min at 15°C (T0). Cells were then moved to 37°C to allow phagocytosis to progress to indicated time periods. Sheep RBCs were opsonized with anti–sheep antibody and 8-µm latex beads and S-FBTs were both opsonized with human IgG for 1 h at RT.

For assays using pharmacological inhibitors, phagocytosis assays were performed using FBTs as described above. 5 min after synchronized attachment, cells were washed to remove unbound FBTs and internalization was allowed to proceed for an additional 15 min at 37°C. Phagocytosis was paused by moving cells to 4°C and external FBTs were immunolabeled using Alexa Fluor 647–conjugated secondary antibody in the cold for 3 min. Cells were washed three times and incubated in pre-warmed media containing the following inhibitors for an additional 20 min at 37°C: 2 µM cytochalasin D, 1 µM jasplakinolide, 2 µM latrunculin B, and 100 µM blebbistatin. External FBTs were immunolabeled again using Alexa Fluor 488–conjugated secondary antibody in the cold for 3 min and cells were then fixed in 4% PFA for 20 min. For treatment with Ly294002, cells were moved to pre-warmed serum-free media containing the inhibitor (100 µM) and incubated at 37°C for 30 min. Phagocytosis assays were performed as described above and particle internalization was measured after 50 min.

For assays using proteases, phagocytic assays were performed as described above. 20 min after the initial FBT attachment, external bacterial were immunolabeled in the cold. Cells were then incubated at 37°C for 20 min in the presence of 1 µM jasplakinolide. After this, cells were either left untreated, treated with 1.0 mg/ml trypsin (Bianco et al., 1975), or treated with 0.2 mg/ml papain (Cambier et al., 1977) for an additional 20 min at 37°C. Cells were then fixed with 4% PFA to assess permeability of DQ-ova or external bacteria were immunolabeled to assess antibody penetration into the T-PCs.

Endosomes and lysosomes were labeled using fluid-phase uptake of tetramethylrhodamine dextran 3 kD, 10 kD, and 70 kD, and DQ-ova. Cells were incubated with the fluorescent probes for 1 h at 37°C, washed, and chased 1 h at 37°C under tissue culture conditions. Phagocytosis assays were performed as described above. For fluorescence labeling of acidic compartments, 20 min after the onset of phagocytosis external sections of the FBTs were immunolabeled in the cold (Alexa Fluor 647–conjugated secondary antibody). After this, the macrophages were incubated with LysoSensor green for 2 min, washed, and moved to precooled microscope stage for imaging.

S-FBTs were opsonized with 1.0 mg/ml human IgG for 1 h at RT. Attachment to RAW cells was synchronized by spinning target particles onto cells at 300 *g* for 5 min at 15°C. Cells were fixed 10 min after initial attachment. To test the effect of pharmacological inhibitors on S-FBT constriction, cells were presented with the target particles in the presence of 1 µM jasplakinolide, 2 µM latrunculin B, and 100 µM blebbistatin, and allowed to engage them in phagocytosis for 10 min before fixation.

Video microscopy of intracellular *L. pneumophila*

Live-cell video microscopy was performed to assess bacterial surival as described previously (Goclaw-Binder et al., 2012; Prashar et al., 2012). 5 h after the initiation of phagocytosis, culture media was removed and replaced with DMEM containing 50 µg/ml gentamycin to kill extracellular bacteria, and phagocytosis was allowed to proceed to indicated times. From previous experiments using FBTs and differential immunostaining, 5 h was sufficient time to allow for complete filament internalization. Cells were moved to a pre-warmed microscope stage (37°C/5% CO_2), infected cells with fully internalized bacteria were identified, and individual cells were followed over time to assess whether the bacteria replicated or were destroyed by the macrophage. Images were acquired at indicated intervals in the presence of gentamycin. Lengths of intracellular bacteria were measured at indicated intervals to quantify elongation.

Scanning electron microscopy

Cells were fixed 20 min after initial attachment and processed as described elsewhere (Silver and Harrison, 2011). In brief, cells were fixed 20 min after initial FTB attachment using 2.5% glutaraldehyde in 0.1 M sodium cacodylate buffer (pH 7.2), followed by post-fixation in 1% OsO_4 for 1 h. Cells were dehydrated in ethanol and sputter-coated with gold. Images were acquired using a scanning electron microscope (JSM 820; JEOL Ltd.).

Immunofluorescence analysis and microscope image acquisition

Confocal images for both fixed and live-cell imaging were acquired using a spinning disc confocal microscope (Quorum Technologies) consisting of an inverted fluorescence microscope (DMI6000B; Leica) equipped with an EM-CCD camera (Hamamatsu Photonics) and ORCA-R^2 cameras and spinning disc confocal scan head, an ASI motorized XY stage, and a Piezo Focus Drive (Quorum Technologies). The equipment was controlled by MetaMorph acquisition software (Molecular Devices). Unless indicated otherwise, all live-cell imaging was performed using a 40× oil immersion objective, 1.3 NA, in DMEM (10% FBS) and an incubator system (Live Cell Instrument; Chamlide). Long-term live-cell imaging was performed at 37°C/5% CO_2. Live-cell imaging in the cold was performed using a precooled microscope stage, maintained at 10°C using a water circulation cooling plate (Live Cell Instrument). A 63× oil immersion objective, NA 1.4, was used for all fixed cell imaging. Cells were fixed in 4% PFA and

coverslips mounted with mounting media (Dako). Unless stated otherwise, all image acquisition was performed using the ORCA-R^2 camera. Image processing, deconvolution (90% confidence interval), 3D reconstructions, and analysis were performed using Volocity software (PerkinElmer), and digital images were prepared using Adobe Photoshop and Illustrator (Adobe Systems, Inc.). Fluorescence intensity measurements to determine S-FBT constrictions were done using ImageJ (National Institutes of Health). Unless indicated otherwise, images shown for fixed cell analysis are deconvolved, merged z-planes.

Statistical analysis

Data shown are mean ± SEM from three independent experiments unless stated otherwise. Fluorescence microscopy was used to perform all quantifications and statistical analysis was performed using two-tailed, Student's *t* test using Prism software (GraphPad Software). 95% confidence interval was used to determine statistical significance and $P \leq 0.05$ was considered to be statistically significant.

Online supplemental material

Fig. S1 shows the phagocytosis of FBTs by cells expressing PM-GFP. Fig. S2 shows FBT containing phagosomes positive for fluorescent dextrans of different molecular weights. Fig. S3 shows that the phagocytic protuberance persists after cells are treated with latrunculin B. Fig. S4 shows that myosin II is not required for the phagocytosis of FBTs. Fig. S5 shows that T-PC and T-PC barrier formation are independent of the opsonin concentration. Video 1 shows the uptake of a FBT by a cell expressing GPI-GFP. Video 2 shows the 3D rendering of a T-PC formed by a GPI-GFP–expressing cell internalizing a FBT. Video 3 shows the dynamics of FBT uptake by a cell expressing GFP-actin. Video 4 shows the fluorescence produced as a result of the proteolytic destruction of an intracellular FBT cross-linked with DQ-ova. Video 5 shows the destruction of an intracellular FBT. Video 6 shows 3D rendering illustrating the constriction of an S-FBT by the actin jacket. Video 7 shows the intracellular replication of a viable *Lp* filament. Video 8 shows an example of the destruction of intracellular *Lp* filament. Online supplemental material is available at http://www.jcb.org/cgi/content/full/jcb.201304095/DC1.

We thank A. Ensminger for sharing the Lp02Δ*dotA* strain and A. Brassinga for sharing the KB288 plasmid. We would like to thank S. Grinstein for sharing the PM-GFP, Rab7-GFP, 2FYVE-GFP, PLCδ-PH-GFP, and PKC-C1δ-GFP constructs and GPI-GFP and GFP-actin stable RAW cells. Voa3-GFP construct was provided by S. Sugita (University Health Network, Toronto, Canada). We thank R.E. Harrison, R. Botelho, A. Brahmendra, R. Garduño, D. Philpott, I. Tattoli, S. Brunt, and D. Bawa for critical discussion of the manuscript.

This work is supported by NSERC and UTSC VPR RCF research grants to M.R. Terebiznik. C. Guyard was supported by the Canadian Institute of Health Research (MOP-102514).

Submitted: 15 April 2013
Accepted: 21 November 2013

References

Aderem, A., and D.M. Underhill. 1999. Mechanisms of phagocytosis in macrophages. *Annu. Rev. Immunol.* 17:593–623. http://dx.doi.org/10.1146/annurev.immunol.17.1.593

Anderson, R.A. Jr., S.A. Beyler, S.R. Mack, and L.J. Zaneveld. 1981. Characterization of a high-molecular-weight form of human acrosin. Comparison with human pancreatic trypsin. *Biochem. J.* 199:307–316.

Araki, N., M.T. Johnson, and J.A. Swanson. 1996. A role for phosphoinositide 3-kinase in the completion of macropinocytosis and phagocytosis by macrophages. *J. Cell Biol.* 135:1249–1260. http://dx.doi.org/10.1083/jcb.135.5.1249

Araki, N., T. Hatae, A. Furukawa, and J.A. Swanson. 2003. Phosphoinositide-3-kinase-independent contractile activities associated with Fcgamma-receptor-mediated phagocytosis and macropinocytosis in macrophages. *J. Cell Sci.* 116:247–257. http://dx.doi.org/10.1242/jcs.00235

Bajno, L., X.R. Peng, A.D. Schreiber, H.P. Moore, W.S. Trimble, and S. Grinstein. 2000. Focal exocytosis of VAMP3-containing vesicles at sites of phagosome formation. *J. Cell Biol.* 149:697–706. http://dx.doi.org/10.1083/jcb.149.3.697

Berger, K.H., and R.R. Isberg. 1993. Two distinct defects in intracellular growth complemented by a single genetic locus in *Legionella pneumophila*. *Mol. Microbiol.* 7:7–19. http://dx.doi.org/10.1111/j.1365-2958.1993.tb01092.x

Bianco, C., F.M. Griffin Jr., and S.C. Silverstein. 1975. Studies of the macrophage complement receptor. Alteration of receptor function upon macrophage activation. *J. Exp. Med.* 141:1278–1290. http://dx.doi.org/10.1084/jem.141.6.1278

Birmingham, C.L., A.C. Smith, M.A. Bakowski, T. Yoshimori, and J.H. Brumell. 2006. Autophagy controls *Salmonella* infection in response to damage to the *Salmonella*-containing vacuole. *J. Biol. Chem.* 281:11374–11383. http://dx.doi.org/10.1074/jbc.M509157200

Björck, P., A. Beilhack, E.I. Herman, R.S. Negrin, and E.G. Engleman. 2008. Plasmacytoid dendritic cells take up opsonized antigen leading to CD4+ and CD8+ T cell activation in vivo. *J. Immunol.* 181:3811–3817.

Botelho, R.J., M. Teruel, R. Dierckman, R. Anderson, A. Wells, J.D. York, T. Meyer, and S. Grinstein. 2000. Localized biphasic changes in phosphatidylinositol-4,5-bisphosphate at sites of phagocytosis. *J. Cell Biol.* 151:1353–1368. http://dx.doi.org/10.1083/jcb.151.7.1353

Botelho, R.J., C.C. Scott, and S. Grinstein. 2004. Phosphoinositide involvement in phagocytosis and phagosome maturation. *Curr. Top. Microbiol. Immunol.* 282:1–30. http://dx.doi.org/10.1007/978-3-642-18805-3_1

Brassinga, A.K., J.M. Kinchen, M.E. Cupp, S.R. Day, P.S. Hoffman, and C.D. Sifri. 2010. *Caenorhabditis* is a metazoan host for Legionella. *Cell. Microbiol.* 12:343–361. http://dx.doi.org/10.1111/j.1462-5822.2009.01398.x

Braun, V., V. Fraisier, G. Raposo, I. Hurbain, J.B. Sibarita, P. Chavrier, T. Galli, and F. Niedergang. 2004. TI-VAMP/VAMP7 is required for optimal phagocytosis of opsonised particles in macrophages. *EMBO J.* 23:4166–4176. http://dx.doi.org/10.1038/sj.emboj.7600427

Bucci, C., P. Thomsen, P. Nicoziani, J. McCarthy, and B. van Deurs. 2000. Rab7: a key to lysosome biogenesis. *Mol. Biol. Cell*. 11:467–480. http://dx.doi.org/10.1091/mbc.11.2.467

Cambier, J.C., E.S. Vitetta, J.R. Kettman, G.M. Wetzel, and J.W. Uhr. 1977. B-cell tolerance. III. Effect of papain-mediated cleavage of cell surface IgD on tolerance susceptibility of murine B cells. *J. Exp. Med.* 146:107–117. http://dx.doi.org/10.1084/jem.146.1.107

Champion, J.A., and S. Mitragotri. 2006. Role of target geometry in phagocytosis. *Proc. Natl. Acad. Sci. USA*. 103:4930–4934. http://dx.doi.org/10.1073/pnas.0600997103

Champion, J.A., and S. Mitragotri. 2009. Shape induced inhibition of phagocytosis of polymer particles. *Pharm. Res.* 26:244–249. http://dx.doi.org/10.1007/s11095-008-9626-z

Champion, J.A., Y.K. Katare, and S. Mitragotri. 2007. Particle shape: a new design parameter for micro- and nanoscale drug delivery carriers. *J. Control. Release*. 121:3–9. http://dx.doi.org/10.1016/j.jconrel.2007.03.022

Chen, K., G.W. Sun, K.L. Chua, and Y.H. Gan. 2005. Modified virulence of antibiotic-induced *Burkholderia pseudomallei* filaments. *Antimicrob. Agents Chemother.* 49:1002–1009. http://dx.doi.org/10.1128/AAC.49.3.1002-1009.2005

Comber, K.R., R.J. Boon, and R. Sutherland. 1977. Comparative effects of amoxycillin and ampicillin on the morphology of Escherichia coli in vivo and correlation with activity. *Antimicrob. Agents Chemother.* 12:736–744. http://dx.doi.org/10.1128/AAC.12.6.736

Cox, D., C.C. Tseng, G. Bjekic, and S. Greenberg. 1999. A requirement for phosphatidylinositol 3-kinase in pseudopod extension. *J. Biol. Chem.* 274:1240–1247. http://dx.doi.org/10.1074/jbc.274.3.1240

Cox, D., J.S. Berg, M. Cammer, J.O. Chinegwundoh, B.M. Dale, R.E. Cheney, and S. Greenberg. 2002. Myosin X is a downstream effector of PI(3)K during phagocytosis. *Nat. Cell Biol.* 4:469–477.

Davis, K.J., P. Vogel, D.L. Fritz, K.E. Steele, M.L. Pitt, S.L. Welkos, A.M. Friedlander, and W.R. Byrne. 1997. Bacterial filamentation of *Yersinia pestis* by beta-lactam antibiotics in experimentally infected mice. *Arch. Pathol. Lab. Med.* 121:865–868.

Dieckmann, R., Y. von Heyden, C. Kistler, N. Gopaldass, S. Hausherr, S.W. Crawley, E.C. Schwarz, R.P. Diensthuber, G.P. Côté, G. Tsiavaliaris, and T. Soldati. 2010. A myosin IK-Abp1-PakB circuit acts as a switch to regulate phagocytosis efficiency. *Mol. Biol. Cell*. 21:1505–1518. http://dx.doi.org/10.1091/mbc.E09-06-0485

Duncan, C., A. Prashar, J. So, P. Tang, D.E. Low, M. Terebiznik, and C. Guyard. 2011. Lcl of *Legionella pneumophila* is an immunogenic GAG binding adhesin that promotes interactions with lung epithelial cells and plays a crucial role in biofilm formation. *Infect. Immun.* 79:2168–2181. http://dx.doi.org/10.1128/IAI.01304-10

Elsliger, M.A., R.M. Wachter, G.T. Hanson, K. Kallio, and S.J. Remington. 1999. Structural and spectral response of green fluorescent protein variants to changes in pH. *Biochemistry*. 38:5296–5301. http://dx.doi.org/10.1021/bi9902182

Flannagan, R.S., G. Cosío, and S. Grinstein. 2009. Antimicrobial mechanisms of phagocytes and bacterial evasion strategies. *Nat. Rev. Microbiol.* 7:355–366. http://dx.doi.org/10.1038/nrmicro2128

Flannagan, R.S., V. Jaumouillé, and S. Grinstein. 2012. The cell biology of phagocytosis. *Annu. Rev. Pathol.* 7:61–98. http://dx.doi.org/10.1146/annurev-pathol-011811-132445

Gillooly, D.J., I.C. Morrow, M. Lindsay, R. Gould, N.J. Bryant, J.M. Gaullier, R.G. Parton, and H. Stenmark. 2000. Localization of phosphatidylinositol 3-phosphate in yeast and mammalian cells. *EMBO J.* 19:4577–4588. http://dx.doi.org/10.1093/emboj/19.17.4577

Goclaw-Binder, H., E. Sendersky, E. Shimoni, V. Kiss, Z. Reich, A. Perelman, and R. Schwarz. 2012. Nutrient-associated elongation and asymmetric division of the cyanobacterium *Synechococcus* PCC 7942. *Environ. Microbiol.* 14:680–690. http://dx.doi.org/10.1111/j.1462-2920.2011.02620.x

Golebiewska, U., J.G. Kay, T. Masters, S. Grinstein, W. Im, R.W. Pastor, S. Scarlata, and S. McLaughlin. 2011. Evidence for a fence that impedes the diffusion of phosphatidylinositol 4,5-bisphosphate out of the forming phagosomes of macrophages. *Mol. Biol. Cell*. 22:3498–3507. http://dx.doi.org/10.1091/mbc.E11-02-0114

Hammer, B.K., and M.S. Swanson. 1999. Co-ordination of *Legionella pneumophila* virulence with entry into stationary phase by ppGpp. *Mol. Microbiol.* 33:721–731. http://dx.doi.org/10.1046/j.1365-2958.1999.01519.x

Harrison, R.E., C. Bucci, O.V. Vieira, T.A. Schroer, and S. Grinstein. 2003. Phagosomes fuse with late endosomes and/or lysosomes by extension of membrane protrusions along microtubules: role of Rab7 and RILP. *Mol. Cell. Biol.* 23:6494–6506. http://dx.doi.org/10.1128/MCB.23.18.6494-6506.2003

Hed, J. 1986. Methods for distinguishing ingested from adhering particles. *Methods Enzymol.* 132:198–204. http://dx.doi.org/10.1016/S0076-6879(86)32008-1

Horvath, D.J. Jr., B. Li, T. Casper, S. Partida-Sanchez, D.A. Hunstad, S.J. Hultgren, and S.S. Justice. 2011. Morphological plasticity promotes resistance to phagocyte killing of uropathogenic *Escherichia coli*. *Microbes Infect.* 13:426–437. http://dx.doi.org/10.1016/j.micinf.2010.12.004

Horwitz, M.A., and S.C. Silverstein. 1980. Legionnaires' disease bacterium (*Legionella pneumophila*) multiples intracellularly in human monocytes. *J. Clin. Invest.* 66:441–450. http://dx.doi.org/10.1172/JCI109874

Isberg, R.R., T.J. O'Connor, and M. Heidtman. 2009. The *Legionella pneumophila* replication vacuole: making a cosy niche inside host cells. *Nat. Rev. Microbiol.* 7:13–24. http://dx.doi.org/10.1038/nrmicro1967

Justice, S.S., D.A. Hunstad, L. Cegelski, and S.J. Hultgren. 2008. Morphological plasticity as a bacterial survival strategy. *Nat. Rev. Microbiol.* 6:162–168. http://dx.doi.org/10.1038/nrmicro1820

Khelef, N., H.A. Shuman, and F.R. Maxfield. 2001. Phagocytosis of wild-type *Legionella pneumophila* occurs through a wortmannin-insensitive pathway. *Infect. Immun.* 69:5157–5161. http://dx.doi.org/10.1128/IAI.69.8.5157-5161.2001

Lawe, D.C., V. Patki, R. Heller-Harrison, D. Lambright, and S. Corvera. 2000. The FYVE domain of early endosome antigen 1 is required for both phosphatidylinositol 3-phosphate and Rab5 binding. Critical role of this dual interaction for endosomal localization. *J. Biol. Chem.* 275:3699–3705. http://dx.doi.org/10.1074/jbc.275.5.3699

Lee, W.L., D. Mason, A.D. Schreiber, and S. Grinstein. 2007. Quantitative analysis of membrane remodeling at the phagocytic cup. *Mol. Biol. Cell*. 18:2883–2892. http://dx.doi.org/10.1091/mbc.E06-05-0450

Lukacs, G.L., O.D. Rotstein, and S. Grinstein. 1991. Determinants of the phagosomal pH in macrophages. In situ assessment of vacuolar H(+)-ATPase activity, counterion conductance, and H+ "leak". *J. Biol. Chem.* 266:24540–24548.

Marathe, S.A., R. Kumar, P. Ajitkumar, V. Nagaraja, and D. Chakravortty. 2013. Curcumin reduces the antimicrobial activity of ciprofloxacin against *Salmonella typhimurium* and *Salmonella typhi*. *J. Antimicrob. Chemother.* 68:139–152. http://dx.doi.org/10.1093/jac/dks375

Mills, I.G., A.T. Jones, and M.J. Clague. 1998. Involvement of the endosomal autoantigen EEA1 in homotypic fusion of early endosomes. *Curr. Biol.* 8:881–884. http://dx.doi.org/10.1016/S0960-9822(07)00351-X

Mitchel, R.E., I.M. Chaiken, and E.L. Smith. 1970. The complete amino acid sequence of papain. Additions and corrections. *J. Biol. Chem.* 245:3485–3492.

Möller, J., T. Luehmann, H. Hall, and V. Vogel. 2012. The race to the pole: how high-aspect ratio shape and heterogeneous environments limit phagocytosis of filamentous Escherichia coli bacteria by macrophages. *Nano Lett.* 12:2901–2905. http://dx.doi.org/10.1021/nl3004896

Molofsky, A.B., L.M. Shetron-Rama, and M.S. Swanson. 2005. Components of the *Legionella pneumophila* flagellar regulon contribute to multiple virulence traits, including lysosome avoidance and macrophage death. *Infect. Immun.* 73:5720–5734. http://dx.doi.org/10.1128/IAI.73.9.5720-5734.2005

Nakada-Tsukui, K., H. Okada, B.N. Mitra, and T. Nozaki. 2009. Phosphatidylinositol-phosphates mediate cytoskeletal reorganization during phagocytosis via a unique modular protein consisting of RhoGEF/DH and FYVE domains in the parasitic protozoon *Entamoeba histolytica*. *Cell. Microbiol.* 11:1471–1491. http://dx.doi.org/10.1111/j.1462-5822.2009.01341.x

Nakao, M., T. Nishi, and K. Tsuchiya. 1981. In vitro and in vivo morphological response of *Klebsiella pneumoniae* to cefotiam and cefazolin. *Antimicrob. Agents Chemother.* 19:901–910. http://dx.doi.org/10.1128/AAC.19.5.901

Nichols, B.J., A.K. Kenworthy, R.S. Polishchuk, R. Lodge, T.H. Roberts, K. Hirschberg, R.D. Phair, and J. Lippincott-Schwartz. 2001. Rapid cycling of lipid raft markers between the cell surface and Golgi complex. *J. Cell Biol.* 153:529–541. http://dx.doi.org/10.1083/jcb.153.3.529

Prashar, A., S. Bhatia, Z. Tabatabaeiyazdi, C. Duncan, R.A. Garduño, P. Tang, D.E. Low, C. Guyard, and M.R. Terebiznik. 2012. Mechanism of invasion of lung epithelial cells by filamentous *Legionella pneumophila*. *Cell. Microbiol.* 14:1632–1655. http://dx.doi.org/10.1111/j.1462-5822.2012.01828.x

Rao, C., H. Benhabib, and A.W. Ensminger. 2013. Phylogenetic reconstruction of the *Legionella pneumophila* Philadelphia-1 laboratory strains through comparative genomics. *PLoS ONE.* 8:e64129. http://dx.doi.org/10.1371/journal.pone.0064129

Raucher, D., T. Stauffer, W. Chen, K. Shen, S. Guo, J.D. York, M.P. Sheetz, and T. Meyer. 2000. Phosphatidylinositol 4,5-bisphosphate functions as a second messenger that regulates cytoskeleton-plasma membrane adhesion. *Cell*. 100:221–228. http://dx.doi.org/10.1016/S0092-8674(00)81560-3

Reiser, J., B. Adair, and T. Reinheckel. 2010. Specialized roles for cysteine cathepsins in health and disease. *J. Clin. Invest.* 120:3421–3431. http://dx.doi.org/10.1172/JCI42918

Ryan, D.M., and D. Monsey. 1981. Bacterial filamentation and in vivo efficacy: a comparison of several cephalosporins. *J. Antimicrob. Chemother.* 7:57–63. http://dx.doi.org/10.1093/jac/7.1.57

Saw, N.M., S.Y. Kang, L. Parsaud, G.A. Han, T. Jiang, K. Grzegorczyk, M. Surkont, G.H. Sun-Wada, Y. Wada, L. Li, and S. Sugita. 2011. Vacuolar H(+)-ATPase subunits Voa1 and Voa2 cooperatively regulate secretory vesicle acidification, transmitter uptake, and storage. *Mol. Biol. Cell*. 22:3394–3409. http://dx.doi.org/10.1091/mbc.E11-02-0155

Scott, C.C., W. Dobson, R.J. Botelho, N. Coady-Osberg, P. Chavrier, D.A. Knecht, C. Heath, P. Stahl, and S. Grinstein. 2005. Phosphatidylinositol-4,5-bisphosphate hydrolysis directs actin remodeling during phagocytosis. *J. Cell Biol.* 169:139–149. http://dx.doi.org/10.1083/jcb.200412162

Sharma, G., D.T. Valenta, Y. Altman, S. Harvey, H. Xie, S. Mitragotri, and J.W. Smith. 2010. Polymer particle shape independently influences binding and internalization by macrophages. *J. Control. Release*. 147:408–412. http://dx.doi.org/10.1016/j.jconrel.2010.07.116

Silver, K.E., and R.E. Harrison. 2011. Kinesin 5B is necessary for delivery of membrane and receptors during FcgammaR-mediated phagocytosis. *J. Immunol,* 186:816–825. http://dx.doi.org/10.4049/jimmunol.1002161

Stauffer, T.P., S. Ahn, and T. Meyer. 1998. Receptor-induced transient reduction in plasma membrane PtdIns(4,5)P2 concentration monitored in living cells. *Curr. Biol.* 8:343–346. http://dx.doi.org/10.1016/S0960-9822(98)70135-6

Sun-Wada, G.H., H. Tabata, N. Kawamura, M. Aoyama, and Y. Wada. 2009. Direct recruitment of H+-ATPase from lysosomes for phagosomal acidification. *J. Cell Sci.* 122:2504–2513. http://dx.doi.org/10.1242/jcs.050443

Swanson, J.A., and S.C. Baer. 1995. Phagocytosis by zippers and triggers. *Trends Cell Biol.* 5:89–93. http://dx.doi.org/10.1016/S0962-8924(00)88956-4

Swanson, J.A., M.T. Johnson, K. Beningo, P. Post, M. Mooseker, and N. Araki. 1999. A contractile activity that closes phagosomes in macrophages. *J. Cell Sci.* 112:307–316.

Tachado, S.D., M.M. Samrakandi, and J.D. Cirillo. 2008. Non-opsonic phagocytosis of *Legionella pneumophila* by macrophages is mediated by phosphatidylinositol 3-kinase. *PLoS ONE*. 3:e3324. http://dx.doi.org/10.1371/journal.pone.0003324

Teruel, M.N., T.A. Blanpied, K. Shen, G.J. Augustine, and T. Meyer. 1999. A versatile microporation technique for the transfection of cultured CNS neurons. *J. Neurosci. Methods*. 93:37–48. http://dx.doi.org/10.1016/S0165-0270(99)00112-0

Tollis, S., A.E. Dart, G. Tzircotis, and R.G. Endres. 2010. The zipper mechanism in phagocytosis: energetic requirements and variability in phagocytic cup shape. *BMC Syst. Biol.* 4:149. http://dx.doi.org/10.1186/1752-0509-4-149

Underhill, D.M., and H.S. Goodridge. 2012. Information processing during phagocytosis. *Nat. Rev. Immunol.* 12:492–502. http://dx.doi.org/10.1038/nri3244

VanderVen, B.C., A. Hermetter, A. Huang, F.R. Maxfield, D.G. Russell, and R.M. Yates. 2010. Development of a novel, cell-based chemical screen to identify inhibitors of intraphagosomal lipolysis in macrophages. *Cytometry A*. 77:751–760.

Vasselon, T., E. Hailman, R. Thieringer, and P.A. Detmers. 1999. Internalization of monomeric lipopolysaccharide occurs after transfer out of cell surface CD14. *J. Exp. Med.* 190:509–521. http://dx.doi.org/10.1084/jem.190.4.509

Vieira, O.V., R.J. Botelho, and S. Grinstein. 2002. Phagosome maturation: aging gracefully. *Biochem. J.* 366:689–704.

Yates, R.M., and D.G. Russell. 2008. Real-time spectrofluorometric assays for the lumenal environment of the maturing phagosome. *Methods Mol. Biol.* 445:311–325. http://dx.doi.org/10.1007/978-1-59745-157-4_20